



Review

# Structural Relaxation, Rejuvenation and Plasticity of Metallic Glasses: Microscopic Details from Anelastic Relaxation Spectra

Michael Atzmon 1,2,\*, Jong Doo Ju 3 and Tianjiao Lei 40

- $^{\rm 1}$  Department of Nuclear Engineering and Radiological Sciences, University of Michigan, Ann Arbor, MI 48109, USA
- <sup>2</sup> Department of Materials Science and Engineering, University of Michigan, Ann Arbor, MI 48109, USA
- Materials Engineering, Testing and Standards (METS), Central Laboratory, Ford Motor Company, Dearborn, MI 48120, USA
- Department of Metallurgy and Materials Engineering, University of Alabama, Tuscaloosa, AL 35487, USA
- \* Correspondence: atzmon@umich.edu

**Abstract:** The lack of periodicity and long-range order poses significant challenges in explaining and modeling the properties of metallic glasses. Conventional modeling of nonexponential relaxation with stretched exponents leads to inconsistencies and rarely offers information on microscopic properties. Instead, using quasi-static anelastic relaxation, we have obtained relaxation-time spectra over >10 orders of magnitude of time for several metallic glasses. The spectra enable us to examine in microscopic detail the distribution of shear transformation zones and their properties. They reveal an atomically-quantized hierarchy of shear transformation zones, providing insights into the effect of structural relaxation and rejuvenation, the origin of plasticity and the mechanisms of the alpha and beta relaxation.

Keywords: metallic glass; shear transformation zone; anelasticity; plasticity



Citation: Atzmon, M.; Ju, J.D.; Lei, T. Structural Relaxation, Rejuvenation and Plasticity of Metallic Glasses: Microscopic Details from Anelastic Relaxation Spectra. *Materials* **2023**, *16*, 0. https://doi.org/

Academic Editor: Paweł Stoch

Received: 19 September 2023 Revised: 11 November 2023 Accepted: 15 November 2023 Published: 27 November 2023



Copyright: © 2023 by the authors. Licensee MDPI, Basel, Switzerland. This article is an open access article distributed under the terms and conditions of the Creative Commons Attribution (CC BY) license (https://creativecommons.org/licenses/by/4.0/).

# 1. Introduction

Amorphous solids, some of which form in natural processes, have been known to humans for thousands of years. Amorphous metallic alloys have only been known in recent decades. Initially formed by vapor deposition [1], they were later formed by solidification from the melt [2], resulting in metallic glasses. The first metallic glasses required high cooling rates to bypass crystallization, typically  $10^6$  °C/s or higher, which limited at least one dimension to  $<10^{-4}$  m. A major breakthrough was achieved when new alloy compositions were discovered that required far lower cooling rates, resulting in bulk metallic glasses with dimensions that exceeded  $10^{-2}$  m [3–5]. As a result, new, especially structural, applications became possible [6,7]. Additional experimental techniques became accessible, e.g., calorimetry in the supercooled liquid region and macroscopic mechanical testing, contributing to enhanced scientific understanding.

Scientists have long been intrigued and challenged by glasses, especially metallic glasses. The periodicity of crystalline solids allows for the use of powerful tools to measure and model their structure and properties. No such tools are available for amorphous solids. Furthermore, the structure and properties of metallic glasses depend strongly on their thermal history, since they relax structurally as they evolve toward a metastable equilibrium state. In addition, rejuvenation by thermal or mechanical means can reverse some of these processes. In equilibrium crystalline solids, in contrast, well-defined point-and extended defects can be introduced by thermal and mechanical treatment, but the base structure at atmospheric pressure is only a function of temperature.

Dislocations, which play a central role in crystalline metal plasticity, are currently well understood [8]. The pioneering work of Sir William Bragg [9] with periodic, two-dimensional bubble rafts allowed him to visualize edge dislocations and their motion,

Materials **2023**, 16, 0 2 of 23

and hypothesize their role in plasticity. Subsequent theoretical work led to a detailed understanding of their properties [8]. Crystal periodicity allows for imaging of dislocations in transmission electron microscopy [10].

In the absence of experimental and theoretical tools that parallel those available for crystalline solids, E. Orowan hypothesized that plastic deformation of disordered solids is accommodated by local, irreversible, rearrangements of clusters consisting of a few atoms/molecules [11]. Because of constraints posed by surrounding atoms/molecules, such rearrangements require thermal activation. Orowan proposed that if such rearrangements are rare and the matrix remains rigid, the memory of the rearranged domains is maintained, leading to anelasticity, i.e., time-dependent mechanical reversibility resulting from backstress upon change in imposed constraints. On the other hand, if the rearranged domains exceed a threshold volume fraction, their memory is lost and permanent deformation, i.e., creep, results. This concept has also been incorporated into more-recent discussions [12–14].

Motivated by Bragg's bubble-raft experiment and Orowan's work, Argon and Kuo [15] created a two-dimensional physical analog of a binary amorphous solid by mixing bubbles of two sizes, each representing an atomic species, reflecting the ease of glass formation in a binary alloy compared to an elemental metal. This glass analog was then subjected to shear in its plane. While dislocations or point defects are readily visible in a periodic bubble raft, observing rearrangements in an amorphous bubble raft required careful tracking of the position of each bubble. At high stress, corresponding to low temperature, they observed local, disk-shaped, rearrangements. At low stress, corresponding to high temperature, they observed shear transformations of equiaxed bubble clusters, with shear values of the order of 0.2. Later experiments in colloidal glass were consistent with these observations [16]. Subsequent studies by numerous authors, e.g., Ref. [17], termed these clusters *shear transformation zones* (STZs). STZ behavior is the focus of the present review. The work included is based on our initial discovery of an atomically quantized hierarchy of STZs [18].

The present review consists of the following:

- A summary of Argon's analysis of the mechanics and thermal activation of STZs.
- Our approach, which consists of (i) quasi-static anelastic recovery experiments that span more than ten orders of magnitude of time and (ii) computational determination of relaxation-time spectra by direct spectrum analysis (DSA).
- Relaxation-time spectra were determined numerically from the strain/time data. These
  provided valuable information on STZ size and property distribution, revealing an
  atomically-quantized hierarchy of STZs.
- Analysis of anelastic relaxation in the nonlinear regime, related to that of Argon and Shi's creep experiments [19], provided an independent determination of the STZ transformation strain. Similar to the dislocation core in crystalline solids, this strain is far larger than the macroscopic yield strain.
- STZ spectra were computed from published dynamic-mechanical data. The results
  provide further, consistent, confirmation of the prior results and their analysis.
- Simple calculations show that stretched exponent fits, commonly used to fit non-exponential relaxation, are of limited utility. In particular, the time constant is ambiguous, and its apparent activation energy is not expected to reflect a specific physical process.
- The systematic error is evaluated for spectrum determination based on measurements conducted at discrete temperature increments and the assumption that the evolution at each temperature is dominated by a single activation free energy.
- Characterization of the details of structural relaxation and induced rejuvenation through their effect on STZ properties shows that these processes cannot be described with the evolution of a single variable.
- Anelastic relaxation spectra were obtained for La-based metallic glasses, some of which exhibit a distinct high-frequency/low-temperature ( $\beta$ ) relaxation. Among the results, the following was found: contrary to suggestions by many authors, the  $\alpha$  and  $\beta$  relaxation correspond to the same mechanism. Both are reversible when the corresponding STZs occupy a small volume fraction. The results also suggest

Materials **2023**, 16, 0 3 of 23

that different elements are involved in slow vs. fast STZs, corresponding to the  $\alpha$  and  $\beta$  relaxation, respectively. Simulations of dynamic-mechanical behavior for experimentally obtained STZ spectra further support the notion that the  $\alpha$  and  $\beta$  relaxation correspond to the same mechanism. That curves obtained at different temperature can be shifted into a single master curve cannot be seen as proof of a single activation energy.

 By comparing metallic glasses that exhibit different degrees of plasticity at similar composition, plasticity is explained in terms of the volume fraction occupied by kinetically active potential STZs.

# 2. Theory of Thermally-Activated Shear Transformation

While STZ analyses in the literature are typically based on an assumption of a single STZ size, our observations, reviewed below, indicate a spectrum of sizes and properties. We therefore modified Argon's kinetic model [12] to express the shear strain rate as a function of shear stress  $\sigma_s$  to account for a spectrum of STZ types, indexed initially with m, each contributing additively to the total shear strain rate [18]:

$$\dot{\gamma}_{m} = 2c_{m}\gamma_{o}^{c}\nu_{G}\exp\left(-\frac{\Delta F_{m}}{kT}\right)\sinh\left(\frac{\sigma_{s}\gamma_{o}^{T}\Omega_{m}}{2kT}\right),\tag{1}$$

where  $\gamma_0^T$  is the transformation shear strain of an STZ unconstrained by the surrounding matrix ( $\approx$ 0.2 [18]), and  $\gamma_0^c = [2(4-5\nu)/15(1-\nu)]\gamma_0^T$  is the constrained value with  $\nu = 0.324$  [20] being Poisson's ratio.  $\nu_G$  is the attempt frequency, k is the Boltzmann constant, and T is the temperature.  $\Omega_m$  is the m-type STZ volume, so  $\gamma_0^T \Omega_m$  is the activation volume.  $\Delta F_m$  is the activation free energy for the shear transformation of m-type STZs [18,19]:

$$\Delta F_m = \left[ \left( \frac{(7-5\nu)}{30(1-\nu)} + \frac{2(1+\nu)}{9(1-\nu)} \overline{\beta}^2 \right) \gamma_0^T + \frac{1}{2} \frac{\overline{\sigma_{STZ}}}{\mu} \right] \mu \gamma_0^T \Omega_m, \tag{2}$$

where the term with  $\overline{\beta}^2$  ( $\sim 1$ ) accounts for the dilatation associated with a shear transformation.  $\overline{\sigma_{STZ}}$  is the shear resistance of STZs,  $\mu$  is the shear modulus, and  $\overline{\sigma_{STZ}}/\mu=0.025$  [21]. This third term in the brackets is negligible compared to the first and second term. Note that in Ref. [12], the pre-exponential factor c is interpreted as the volume fraction occupied by potential (or fertile) STZs, i.e., atomic clusters capable of undergoing a shear transformation. In the present work, the  $c_m$  are resolved by STZ type, m, and obtained from experiment, as shown below. It is noted that in the notation used, overlapping potential STZs are counted multiple times. Equation (1) is valid as long as only a small fraction of them undergoes shear transformations.

# 3. Experiments and Spectrum Determination

The experimental basis for the presently reviewed work is the room-temperature measurement of quasi-static anelastic relaxation (Figure 1) over a wide range of time constants. The simple exponential decay for each time constant in the spectrum facilitates the data analysis, as compared with commonly used dynamic-mechanical analysis (discussed below). For short time constants, ~1.5  $\times$  10 $^{-3}$ –200 s, using a nanoindenter at fixed force to monitor the displacement of a cantilever (Figure 1a) as a function of time provided the strain evolution. For long time constants, up to ~6  $\times$  10 $^{7}$  s, instrumented measurements pose stability challenges. Instead, therefore, 20–40 µm thick ribbon samples were constrained for 2  $\times$  10 $^{6}$  s around a mandrel at a fixed radius of curvature; subsequently, their radii of curvature were monitored as a function of time in a stress-free state. Except for the early study of Al<sub>86.8</sub>Ni<sub>3.7</sub>Y<sub>9.5</sub> [18], the sample curvature determination was performed using an automated fit to its image. Based on the confirmed linearity of the relaxation process, the strain and stress at any distance from the neutral midplane were calculated as a function of time. The strain at the surface is used in all reported data.

pose stability challenges. Instead, therefore, 20-40 µm thick ribbon samples were constrained for 2 × 106 s around a mandrel at a fixed radius of curvature; subsequently, their radii of curvature were monitored as a function of time in a stress-free state. Except for the early study of Alsos Ni3.7Y9.5 [18], the sample curvature determination was performed using an automated fit to its image. Based on the confirmed linearity of the relaxation process, the strain and stress at any distance from the neutral midplane were calculated as a function of time. The strain at the surface is used in all reported data.

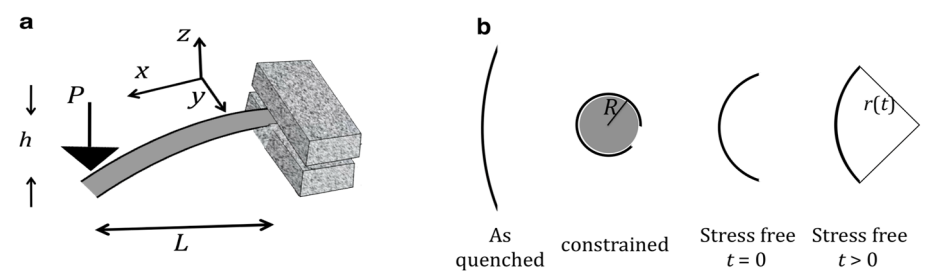


Figure 1. Measurement techniques. (a) Cantilever method. The displacement h is monitored from 1. Measurement techniques. (a) Cantilever method. The displacement h is monitored as a same and the first of time at a fixed load, h. The instantaneous displacement is the elastic component, h is the elastic component h is the elastic component, h is the elastic component (b)aMandrelenethe 4nEbsampele was constanied to 22×100°s at varying radii, after which the radius of curvature was manitural desa function of time in a stress descreon dition tibap Reprenductor (I und Pa; JaDe, JangND ankpanapatanéna MoranAtemiaally igalilytipedrhieearchiyrafelyearfulaesformationzonies izonenetallingtaskic/glapp//.Phyp/.2014s.12011w10PperithissionissionPoPublisRudglishing [18].

While knowledge of the spectrum allows for an explicit expression of the strain evolution, the reverse is not true – the spectrum is only implicitly determined. Therefore, the spectra-reeded to be determined an merically, we insumbation in an avairant enectrupe and m sin 1973 i F 1227 . the otra in time and tame Jaxation et invarions the computed using GOOT TISING reconstruy, a kase hore y alchayer to psolde moderno lesse a formation of the same and the same and the contract of the same and the sa yariations in the solution of the elimination, unply sign bracks with fellowies at a incline. functions transcripted transcripts the renalisetic time-dop and entertain, based open linear scalid, madel (see believe): soil Font de mondrelloxperiment, the (thatigret experiment, experimen where  $\xi_{\rm exp}$  and the  $\xi_i$  are fitting parameters. The former represents possible processes with  $\pm t_{\rm exp}^{\rm exp} = t_{\rm exp}^{\rm exp}^{\rm exp} = t_{\rm exp}^{\rm exp}^{\rm exp} = t_{\rm exp}^{\rm exp}^{\rm exp}^{\rm exp} = t_{\rm exp}^{\rm exp}^{\rm exp}^{\rm exp}^{\rm exp}^{\rm exp$ 

#### 4. An Atomically Quantized Hierarchy of STZs [18]

4. An Atomically Quantized Hierarchy of STZs [18] These original experiments were performed with  ${\rm Al}_{86.8}{\rm Ni}_{3.7}{\rm Y}_{9.5}$  metallic glass ribbons. The energiand experiments repeate transfer with Alean (1) was tallicustes aid to me tempteratmential connariaments on the abuse lastification in a time (to), 80 % 1070 yita redeat violen its copyrate it shalter. Construction was a superior of the construction of  $\mathfrak{A}_{e^{\prime}}$  for the construction of the constr osigina canapeailt the hamples. Fagure 2veoronalized by lieatifor treatetal menabul padiiessed toccinnstraitinharsacgidae. Alhisuticactoinsidepintidating that flicanthastiteprocesse partile absolisathe eegippe. Thiskohesstily isooppolits also assphysticanthat significaint priedide laculosekthe pstroople/thinaltriespiective are Veals at inarphied tilpde trioneignoinistant tyrigeby brand traken ophistic Veisoral ery. Figure 3 shows representative  $\varepsilon_{an}(t)/\varepsilon_{el}^0$  curves, along with corresponding computed spectra,  $f(\tau)$ , for the cantilever (Figure 3a) and mandrel (Figure 3b) experiments. Fits obtained with different numbers of fitting points,  $N_1$  and  $N_2$ , demonstrate the consistency of spectrum computation.

inspection reveals that multiple time constants govern the anelastic recovery. Figure 3 shows representably expected ( $t_1$ )/ $t_2$  each that  $t_3$  multiple time constants govern the anelastic recovery. Figure 3 shows representably expected that  $t_3$  multiple time constants govern the anelastic recovery. Figure 3  $f(\tau)$ , for the cantilever (Figure 3) and  $t_3$  for the cantilever (Figure 3) and  $t_4$  fo

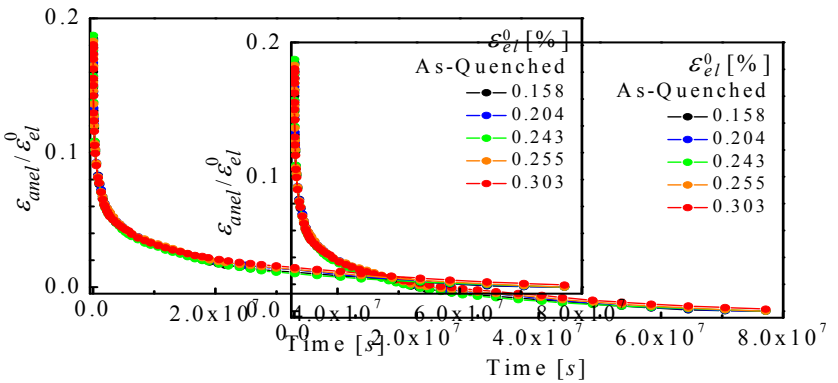


Figure 2. Anelastic strain evolution following equilibration at different mandrel radii. The strain is normalized by the **figure 3.** Anelastic introduction of the control of the control

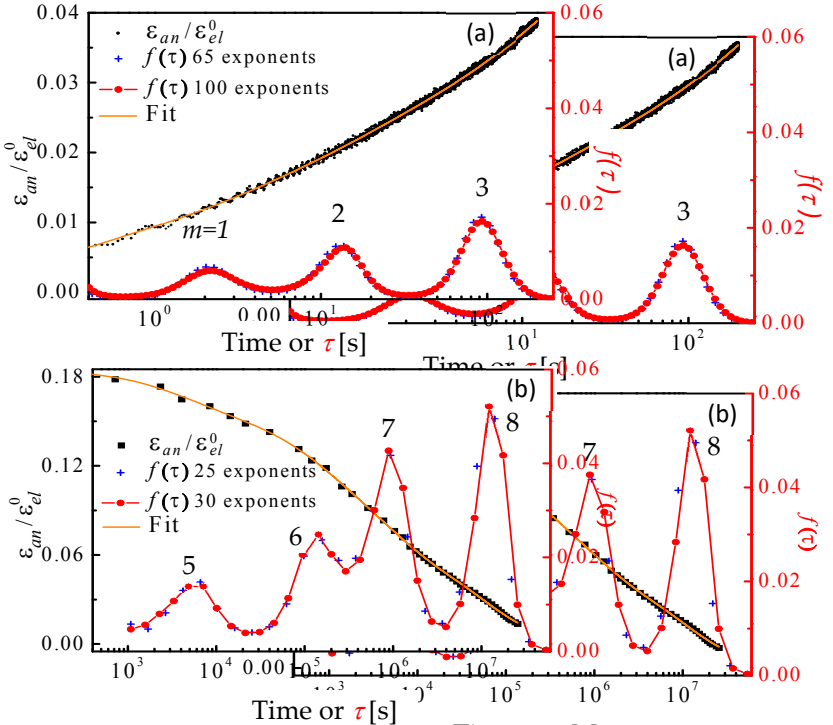


Figure 3. Sample relaxation curves and corresponding relaxified times pectra. (a), Cantilever measurement, performed in a stress of the control of the cont

Surprisingly, the spectra in Figure 3 consist of distinct peaks, indexed with m. This discovery motivated substingly the spectral in Figure 3 consist of distinct peaks, indexed with m. This spring (effective discovery motivated spectral in Figure 3 consist of distinct peaks, indexed with m. This spring (effective discovery motivated spectral in Figure 3 consist of distinct peaks, indexed with m. This spring (effective discovery motivated spectral in Figure 3 consist of distinct peaks, indexed with m. This spring (effective discovery motivated spectral in Figure 3 consist of distinct peaks, indexed with m. This spring (effective discovery motivated spectral in Figure 3 consist of distinct peaks, indexed with m. This spring (effective discovery motivated spectral in Figure 3 consist of distinct peaks, indexed with m. This spring (effective discovery motivated spectral in Figure 3 consist of distinct peaks, indexed with m. This spring (effective discovery motivated spectral in Figure 3 consist of distinct peaks, indexed with m. This spring (effective discovery motivated spectral in Figure 3 consist of distinct peaks, indexed with m. This spring (effective discovery motivated spectral in Figure 3 consist of distinct peaks, indexed with m. This spring is the spectral in Figure 3 consist of distinct peaks, indexed with m. This spring is the spectral in Figure 3 consist of distinct peaks, indexed with m. This spring is the spectral in Figure 3 consist of distinct peaks, indexed with m. This spring is the spectral in Figure 3 consist of distinct peaks, indexed with m. This spring is the spectral in Figure 3 consist of distinct peaks, indexed with m. This spring is the spectral in Figure 3 consist of distinct peaks, indexed with m. This spectral in Figure 3 consists of distinct peaks in m and m and m and m are spectral in Figure 3 consists of distinct peaks in m and m are spectral in m a

$$\tau_m = \frac{3\eta_m'}{E_m'} \,, \tag{3}$$

dashpot (effective viscosity  $\eta'_m$ ) in parallel (Figure 4, top). Under zero or fixed stress, Voigt unit relaxes exponentially with a time constant

$$\tau_m = \frac{3\eta_m'}{E_m'},$$

6 of 23 Materials 2023, 16, 0

> where the factor of 3 accounts for the conversion of uniaxial to shear viscosity. The u linear viscosity is valid when the sinh term in Equation (1) is linear in the stres confidence the factor of 3 accounts for the conversion of uniaxial to shear viscosity. The distribute work of linear viscosity is valid when the sinh term in Equation (1) is linear in the stress, as time constants however than the constraining of uniaxial to shear in the stress, as time constants however than the constraining of uniaxial penalty and constant with otheinandristans phinter that mepresents rting that tied the viorical eldingrium with each

other and the spring that represents the elastic behavior, yielding  $E'_m = \frac{\varepsilon_{el}}{\varepsilon_m^0} E_0,$   $E'_m = \frac{\varepsilon_{el}}{\varepsilon_0^0} E_0,$  (4) where  $E_0$  (see Figure 4) is the sample's higher-frequency Young's modulus. By definition where  $E_0$  (see Figure 4) is the sample's high-frequency Young's modulus. By definition,  $\varepsilon_m^0 = \varepsilon_{e,l}^0 \times \int_m f(\tau) dln\tau$ ,

is the contribution of Voigt Unit m to the strain, with integration over peak m in spectrum ditismented direction the spectrum in Tigure the their reason descriped use 8 does reflect mechanical equilibrium because the corresponding time constant is longer than the constraining time. reflepermechatikealted that britans bectruse this earles board myntener ebustant lie songer than

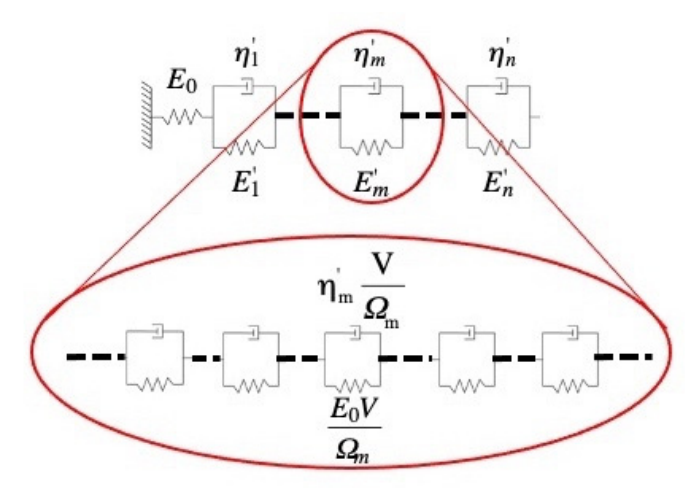


**Figure 4.** Top: linear solid model: n anelastic processes act in series, each represented by a Voigt **Figure 4.** Top: linear solid model: n anelastic processes act in series, each represented by a unit. m-type sites are associated with Young's modulus of E' and viscosity  $f'_{m'}$  both effective materials are associated with Young's modulus of E' and viscosity  $f'_{m'}$  both effective materials. unitquantypes sites rereversely proposition of the sendity is gosity to the sendity to the sendity is gosity to the sendity is gosity to the sendi quantities that are inversaly propartional to the two lumb traction as the spesites to by in the high quency: Young sanodulum Bottom, allustration reptha contribution of anchanty pastize to Voigt m. Respective of the arm dust bull at language in laractific glass Atzapon Phys. 2011 at conically equacitized hiera of sheathfabishing thin zones in a metallic glass. J. Appl. Phys. 2011, 109. with permission of

Publishing [18]. The centroids of the spectrum peaks in Figure 3 are the time constants  $\tau_m$ , and their areas yield  $E'_m$  according to Equation (4). Then, using Equation (3), the  $\eta'_m$  values are of the central destriction of the control of the constant of t yieldeflyticaccondingviscoliquation  $\frac{\sigma(4)}{n}$  whehen, is using elsquations (3)), the day potatues are tainedit Nosuralge tresults agrebe fell hied doubting lones piters ive law. (Equation (1)) using the inition of linear viscosity  $\dot{\gamma}_m = \frac{\sigma_s}{\eta_m'} \dot{\varepsilon}_m^{\nu}$  where  $\sigma_s$  is the net shear stress on the dashpot in m. Straightforward algebra [18]  $\dot{\gamma}_m$  is  $\dot{\gamma}_m$  in  $\dot{\gamma}_m$  i

The lower part of Figure 4 illustrates the converge upon the strict of the strict of

Based on the equations above, with linearized sinh in Equation (1), the properties The lower part of Figure 4 illustrates the contribution of each individual type-*m* pote of each *potential* STZ type, *m*, are plotted in Figure 5. Using literature data for the elastic STZ this was the interpretable that the perpension of the state of

atBassedobumthof eduia flignsealbothe, ewithirlineaisized Isinhe ina Epperation the lexythree properti each potential STZ type, m, are plotted in Figure 5. Using literature data for the el constants, the volume of type-m STZs,  $\Omega_m$ , is obtained and displayed, normalized by atomically-quantized hierarchy of STZs – the spectrum peaks correspond to STZs that consist of n=14,..., 21 atoms. The dominance of a single element, Al, likely facilitates the resolution of this hierarchy. The activation free energies corresponding to this STZ hierarchy,  $\Delta F_n$ , range from 0.85 to 1.26 eV (Equation (2), Figure 5f).

Later experiments [27], conducted at longer duration (constraining time  $4.4^{\circ} 2^{\circ} 10^{\circ}$  s and anelastic recovery for  $1.1 \times 10^{\circ}$  s) further confirmed the hierarchy, showing the signature of STZs consisting of 22 atoms. The  $c_n$  obtained allowed for modeling the size-density instruction (1): was asshabled third she she death the obtains a stiff of the size of the she density instruction (1): was asshabled third she she death the specific poissones and durable free was the specific poissones and the specific poissones and the specific poissones and the specific poissones and the specific poissones are she shall be specified as the specific poissones and the specific poissones are specified by the specific poissones as the resolution of this hierarchy. The activation free energies corresponding to this STZ volume is shared dynamically within the STZ on a time scale required for shear transformation.

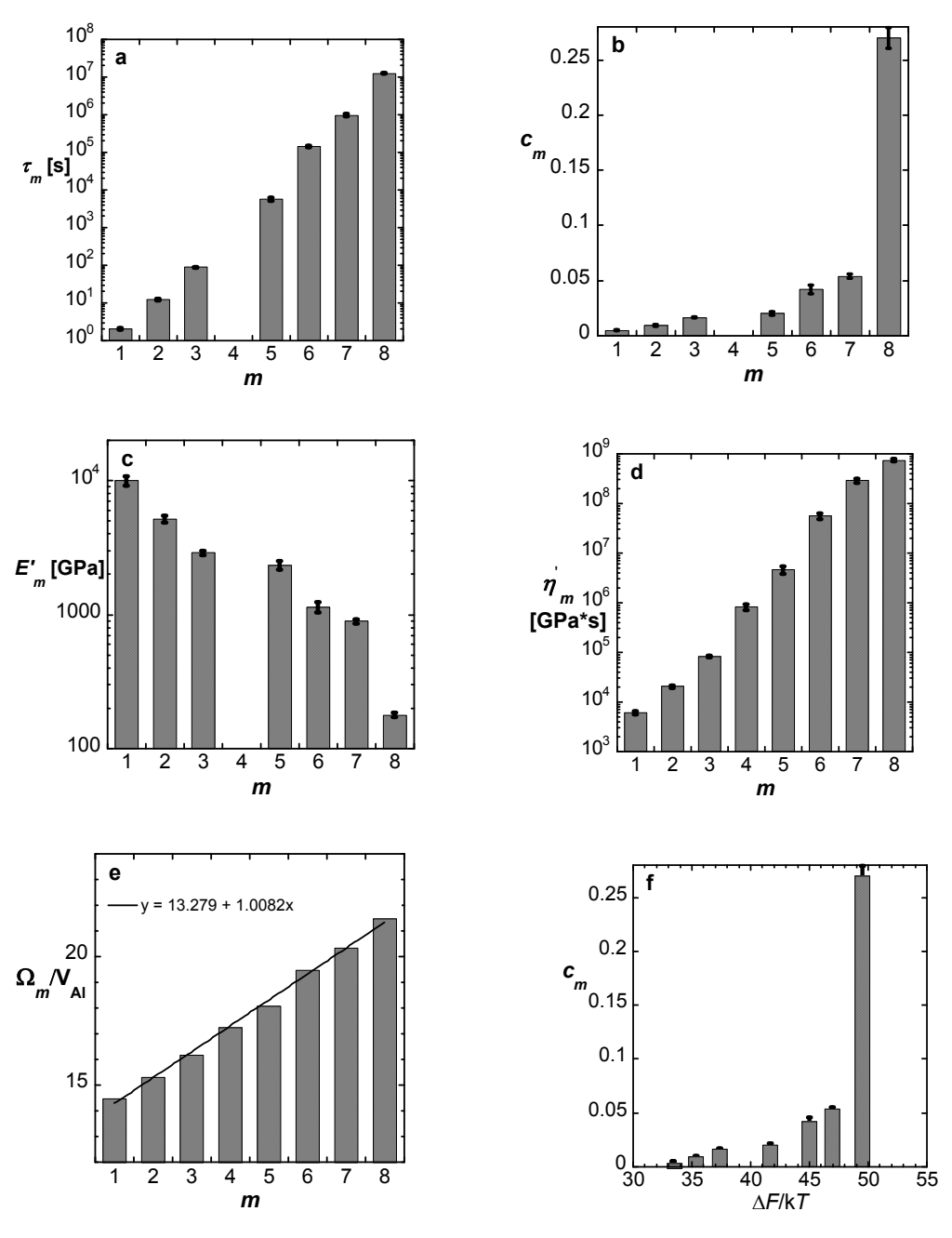


**Figure 5.** Al<sub>86.8</sub>Ni<sub>3.7</sub>Y<sub>9.5</sub>: Calculated properties of the respective anelastic processes m = 1–8. (a) Time constants. (b) Volume fraction of *potential* STZs. (c) Effective macroscopic Young's modulus. (d) Effective macroscopic viscosity. (e) STZ volume in units of atomic volume of Al, V<sub>AI</sub> = 16.6 × 10<sup>-30</sup> m<sup>3</sup>. Values for m = 4 were obtained by interpolation. (f) Volume fraction of *potential* STZ as a function of  $\Delta F/kT$ . The error bars are the standard deviation of the mean, obtained by averaging over multiple measurements. Reproduced from Ju, J.D.; Jang, D., Nwankpa, A; Atzmon. M. An atomically quantized hierarchy of shear transformation zones in a metallic glass. *J. Appl. Phys.* **2011**, 109. with permission of AIP Publishing [18].

The activation volume for shear transformation is the product of the transform strain  $\gamma_0^T$  and STZ volume  $\Omega_m$ . They cannot be determined independently from the above because only the product  $(\gamma_0^T)^2 \Omega_m$  appears in the (linearized) sinh term in tion (1) and in Equation (2), recalling that the third term in Equations(2)3is negl Therefore,  $\gamma_0^T$  had been estimated from experiments conducted in colloidal glass [1 from molecular dynamics simulations [29,30],  $\gamma_0^T \approx 0.2$ , which affects the resulting of  $\Omega_m$ . After experiments [37] conducted at longer duration (for a straining time 4.54 in the stortlinear range and stic recovery for  $1.1 \times 10^8$  s) further confirmed the hierarchy, showing the signature of the sinh term of Equation (1). Such analysis was carried out by Argon and Shi [37] of STZs consisting of 22 atoms. The  $c_n$  obtained allowed for modeling the size density nonlinear of each data und complement the dinear results upresented above reve conc nonlinear an elastic relatation apaperiments on Administration of the strict of the st snfaller frankelten edistribution, of 35% ratio up to ( varied only slightly with size, as  $\mu^{0.22}$  [27]. This weak dependence is expected if free volume compared with 0.00303, for the prior experiments in the linear regime. For the res stress, the sinh term in Equation (1) is nonlinear. The volume fraction occupied by S still The all and the STZs can be considered to the STZs can be co isolate The Michigan volumed fourthour voristoinne time is the product of the trins three stimple geo following brief constraint: The They cannot be determined independently from the data above because only the product  $(\gamma_1^T)^2\Omega_m$  appears in the (linearized) sinh term in the stress-free curvature at t=4 x  $10^6$  s after the release of the constraint, is show Equation (1) and in Equation (2), recalling that the third term in Equation (2) is negligible. function of the abstice constraining strain in Figure to for hoth the son fine ar and linean datacuAst stychnaigsoimtulatitims (29th), fast STZ sylhadren fielasthd, resudtitlge haugest STZ vafe@wAffindepandent determination of xa from its experiments in the nonlinear regime

of the sinh term of Equation (1). Such analysis was carried put by Argon and Shi, 191 for nonlinear equations to these data, yo = 0.17 is obtained. By computing the nonlinear ereep data. To complement the linear results presented above, we conducted fit sensitivity as this value the inandom arror is determined to be ±3 by using before fit nonlinear training the total periments on As Strike determined to be ±3 by using before fit sensitivity as the strain of the sachthasulting posterior in the sample growth of the sachthasulting posterior than expose entire the inalysis in 184 for 2, as sinh term in Equation (1) is proplinear. The real results of the sinh term in Equation (1) is proplinear. The real results of the STZs can be considered at 187 by 187 as that STZ interactions are negligible and the STZs can be considered matroscopic yield strain observed in metallic glasses, 0.036, 31. An important para isolated. Yield was ruled out by verifying the absence of change in the sample geometry crystalline solids helps. The strain the strain ineadislocate is of the value of 14 by 184 the strain of the tals is inclined with the strain ineadislocate settles strain time, the fast STZs have relaxed and the largest STZs activated, with a point in time, the fast STZs have relaxed and the largest STZs activated, with a 182, dominate the relaxation behavior.

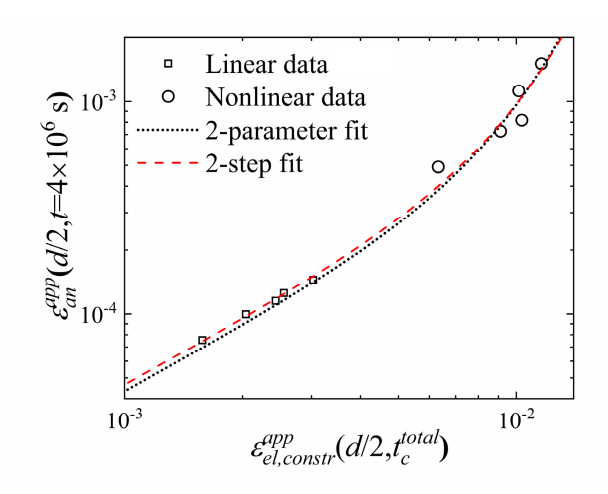


Figure 6: Alphanie it as a sparent elastic strain after train offst runned reinax ation for f ≠ 106 s as function as function of the apparent elastic strain at the end of the constraining period for varying constraining radii. B radii. Both are computed for the sample surface from the curvature. Each symbol represents one sample. Linear data are from Ref. [18]. Deviation from linearity occurs at high strain. Comparison between the two-parameter fit (dotted line) and two-step fit (dashed line) (see Ref. [28]): the latter yields a better fit for the small-strain data than the former. Reproduced from Lei, T.J.; Atzmon, M. Activation volume details from nonlinear anelastic deformation of a metallic glass. J. Appl. Phys. 2019, 126, 185104, with permission of AIP Publishing.

Materials **2023**, 16, 0 9 of 23

Fitting the nonlinear equations to these data,  $\gamma_0^T = 0.17$  is obtained. By computing the fit sensitivity to this value, the random error is determined to be  $\pm 3\%$ . As before for the  $\Omega_m$ , this small error is due to the fact that  $\gamma_0^T$  appears in the exponent in Equation (2). The value obtained,  $\gamma_0^T = 0.17$ , is reasonably close to the value assumed in the analysis in Ref. [18], 0.2, as summarized above. It is much greater than the universal, low-temperature, macroscopic yield strain observed in metallic glasses, 0.036 [31]. An important parallel to crystalline solids helps illustrate this difference in magnitude: the strain in a dislocation core is of the order of 1, yet the yield strain in metals is below 0.01. It is worth noting that in some studies, equating the transformation strain to the yield strain resulted in unphysically large STZ sizes being backed out from the data [32,33].

### 6. Dynamic-Mechanical Analysis [34]

In the analysis of quasi-static data obtained at room temperature, the temperature dependence of the strain rate had to be assumed, see Equations (1) and (2). Measurements at varying temperature involve stability challenges because of the long time involved. While fitting frequency-dependent dynamic-mechanical data poses challenges, it enabled us to carry out a direct evaluation of the temperature dependence.

The analysis methodology to be used was evaluated by simulating the loss modulus [26],  $E''_s(\omega)$ , as a function of frequency  $\omega$  for an input spectrum of time constants,  $f^a(\tau)$ , based on Ref. [18]:

$$E_s''(\omega) = E_0'' \times \int f^a(\tau) \frac{\omega \tau_i}{1 + (\omega \tau_i)^2} dln\tau. \tag{7}$$

 $E_{\rm s}''(\omega)$ , plus added noise, was then fitted with

$$E''(\omega) = \sum_{i=1}^{N} f_i \frac{\omega \tau_i}{1 + (\omega \tau_i)^2},$$
(8)

where the time constants  $\tau_i$  are logarithmically spaced, N = 70 and the  $f_i$  are fitting parameters representing a discrete best estimate of the spectrum. Iterative fits were repeated for increasingly tighter target tolerance values [34] for each of the multiple simulated spectra. It was found that input spectra were most-accurately recovered for the tolerance value at which  $R^2$ , the coefficient of determination, began to increase. This tolerance value was used as the best-fit criterion when analyzing the experimental data.

Because of the steep variation of the loss modulus with temperature, curves measured as a function of frequency, acquired at multiple temperatures, lend themselves better to fitting the model than the more common curves obtained as a function of temperature. Therefore, the extensive data of Ref. [35], obtained for  $Zr_{46.8}Ti_{13.8}Cu_{12.5}Ni_{10}Be_{27.5}$ , were used in the analysis. The fits and corresponding spectra are shown in Figure 7. The time constants obtained from each peak are shown in Arrhenius plots in Figure 8 as a function of temperature. The goal was to obtain simultaneous fit lines for all STZ sizes, based on an atomically quantized hierarchy of STZs. For each trial STZ size n, the time constant was expressed as a function of temperature based on the theory reviewed above:

$$\tau_n = \frac{3kT}{2\mu(1+\nu)\nu_G \gamma_o^c \gamma_0^T \Omega_n} \exp\left(\frac{\Delta F_n}{kT}\right),\tag{9}$$

with  $\Delta F_n$  given by Equation (2).

Since the data [35] were obtained both below and above the glass transition temperature,  $T_g$ , and the shear modulus varies significantly with temperature in the latter range, its approximate linear temperature dependence above  $T_g$  was included in the fits [36–39]. They were carried out simultaneously for all values of T and T. The main challenge was determining which set of data points corresponded to the same STZ size, T0, within a multi-T1 simultaneous fit. Several plausible groupings were attempted each below and above T1. The only combination of such sets that yields continuity and the same T2 values across T3 is that shown in Figure 8a. The resulting T2 values range from 25 to 33, with

Materials 2023, 16, 0 10 of 23

corresponding activation free energies of 1.75–2.3 eV. These results are consistent with those of Ref. [18], further confirming them and the model used. These higher values of n, compared with 14–22 at room temperature in Ref. [18], are expected since the spectra increase monotonically and larger STZs become active with increasing temperature.

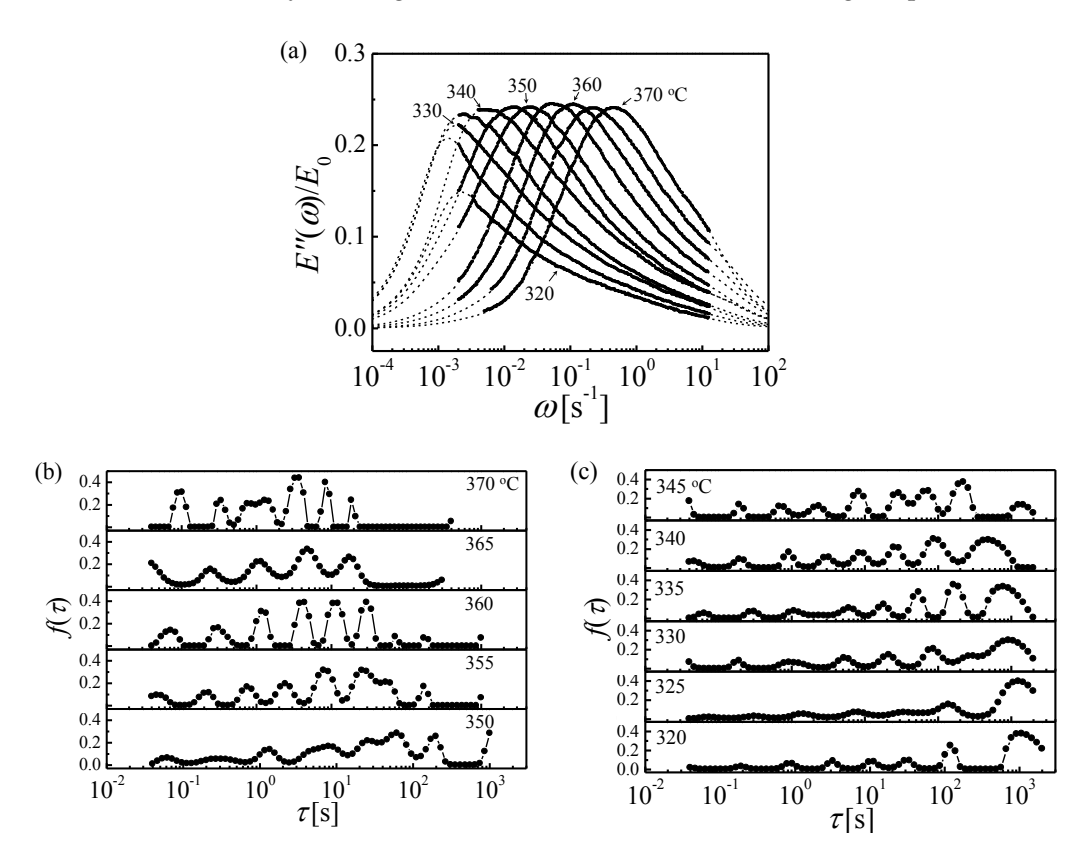


Figure 7. Zrfigfins 3.(H) Distile Bezoss fas digitis of when Denvetuli (16,5) syith a Satelited (hour spectrals above obtained from the selections and reprinted by the exatomistic analysis of the exatomist analysis of the exatomistic analysis of the exat

It is instructive its tevativate avaluate at the single frame same super puritors principle ple [40–43]. One 431 in the first instructions is that for a way the single is the single in the single is the single is the single in the single is the single in the single is the single in the single in the single is the single in the single in the single in the single is the single in the single i

$$\Delta \ln(\omega_i) = \frac{\Delta E_a}{kT} \ln \left(\frac{1}{T_i}\right) = \frac{\Delta E_a}{T_k T_f} \left(\frac{1}{T_i} - \frac{1}{T_{ref}}\right)$$
(10)

will coincide'il·la spiglelmaister ceitele white the cutve meabureler at the reference  $T_{ref}$ . Using these requiredeshifting these required shifting these required shifting these requiredeshifting the shifting these required shifting the shifting these required shifting the shifting the

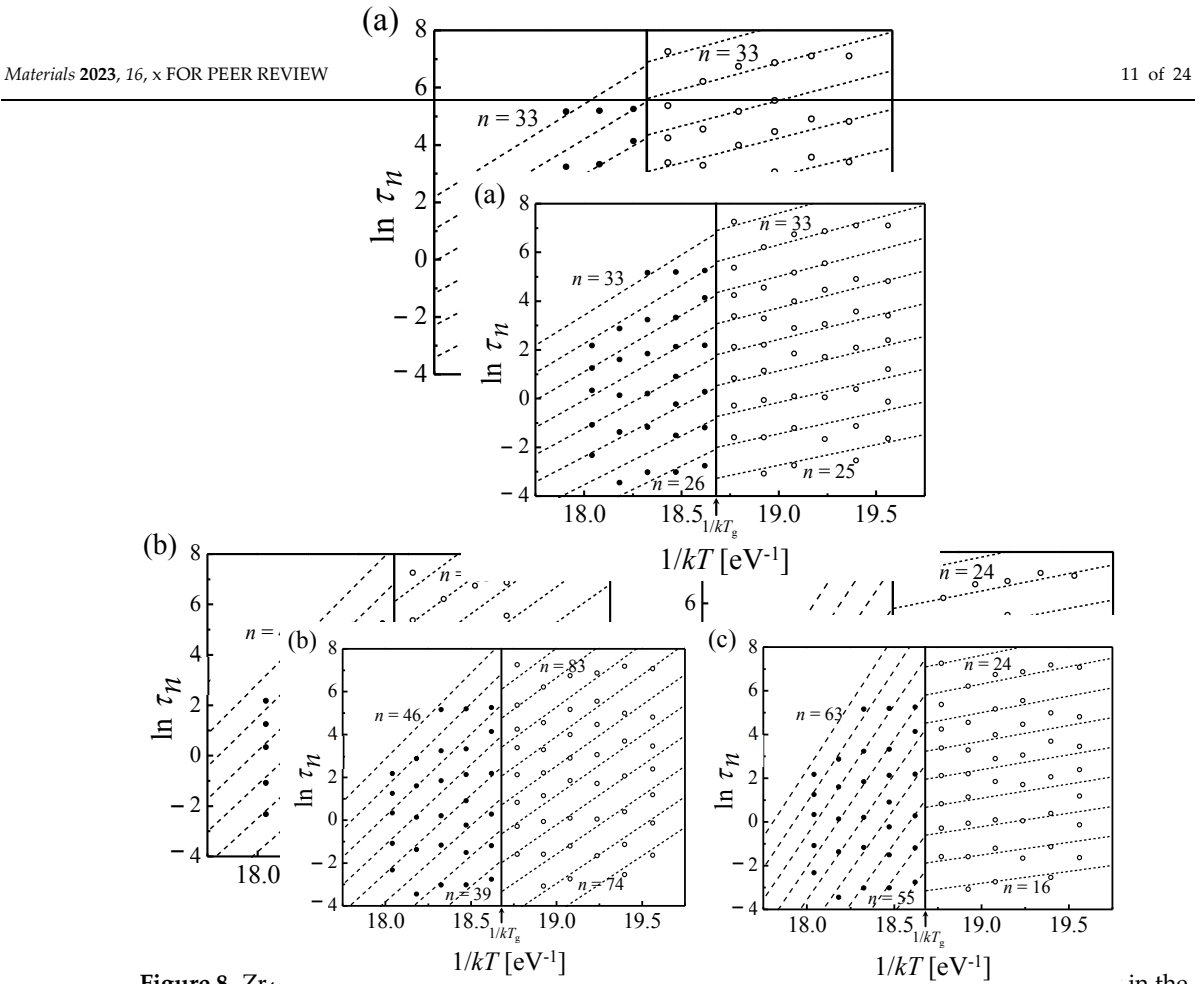
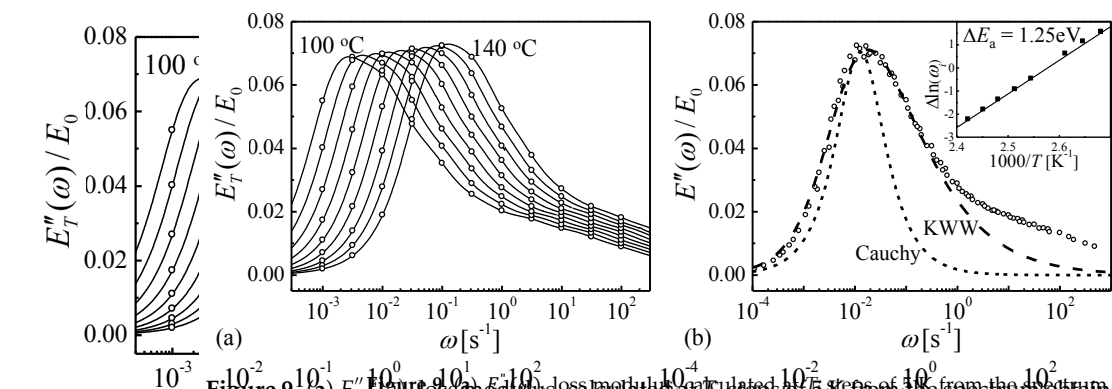


Figure 8. Zr<sub>46.0</sub> 113.0 Ca<sub>12.3</sub> trum the median of the respective peak in the relaxation-time spectra of relaxation-times spectra of relaxation-times in the relaxation spectra of relaxation-times in the relaxation spectra of relaxation-times in the relaxation spectra of relaxation spectr



(a)

Figure 9. (a) Entroyed on Early solutions, early study of the property of the spectrum of the restriction of the study of the stud

Materials 2023, 16, 0 12 of 23

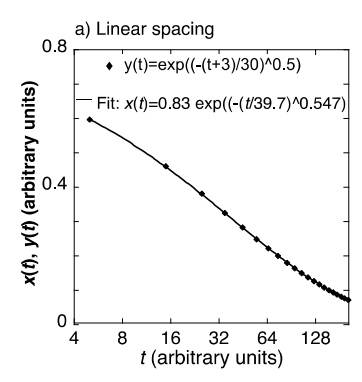
#### 7. The Stretched Exponent [45]

This section further rationalizes the need to compute relaxation-time spectra from the anelastic relaxation data described above. Many processes in nature exhibit exponential decay, which takes place when the rate of change of a variable is proportional to the variable itself. However, one often encounters deviations from this ideal behavior. Early on, Kohlrausch [46] proposed describing the electrostatic discharge of a capacitor as a function of time with a stretched exponent,

$$x(t) = x(0)\exp\left(-\left(t/\tau_{s}\right)^{\beta}\right),\tag{11}$$

with  $\tau_s$  and  $\beta$  being constants and x(0) being the initial charge. Currently, many studies of non-exponential relaxation in disordered materials employ this expression, referred to as Kohlrausch-William Watts (KWW) [47,48]. This time dependence has also been used to derive the behavior in the frequency domain [47]. The expression, which often provides good fits, is phenomenological in most cases, with few exceptions for which it results from a mechanistic model [49–51], usually near or above the glass transition. Despite the phenomenological nature of Equation (11), it is often assumed to represent a physical process [52–60], leading to conclusions that are difficult to support. Examples among these are the KWW fitting of the dielectric loss or the loss modulus in glass. Deviations from the fitted KWW curve at high frequency, also seen in our  $E''(\omega)$  calculated from experimental spectra, are interpreted by some authors as resulting from a separate relaxation mechanism. This amounts to assuming a priori that the behavior should correspond to the spectrum of time constants consistent with KWW behavior. However, as our present results and analysis show, a single mechanism, namely shear transformations, can explain the behavior without relying on this often unsupported restriction. The very interpretation of  $\tau_s$  as a time constant is problematic because of an internal inconsistency: simulated data points, based on a stretched exponent, shifted by 10% of  $\tau_s$ ,  $\exp(-((t+3)/30)^{0.5})$ , were fitted with an unshifted stretched exponent (Figure 10). The fitting parameters depend on the range of t values and the manner in which the points are spaced on the t axis. However, as shown in Figure 10, similar results are obtained for linear (a) and logarithmic (b) spacing, where the former gives greater weight to long time values. Both yield good fits with similar fitting parameters. Remarkably, the  $\tau_s$  values obtained are higher by >30% than the value of 30 used to simulate the data points. This is a result of the fact that, unlike for a simple exponent, the relative rate of change of the stretched exponent is not constant in time. The common assumption that the temperature dependence of  $\tau_s$ , however obtained, can yield an activation energy [53,57]

Materials 2023, 16, x FOR PEER REVIEW is therefore not supported. For these reasons, the presently reviewed work is based on spectrum determination from the data without prior assumptions.



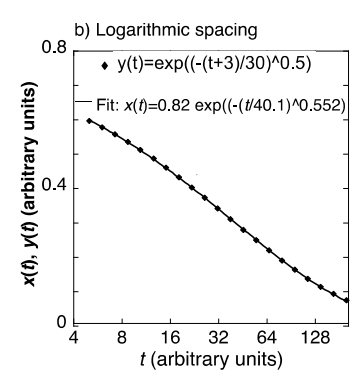


Figure 100 A hymothetical time damay dept and ptily a described as a stretched exponent with a small shiftstrift ( $\psi(t)$ )cioperiscitteles)itts afitteeritteithum neurskiitteelt stilltenedien ( $\psi(t)$ ), Equation (1), line). Linearly spaced time points; (b) Logarithmically spaced time points. Significantly different  $\tau$  and  $\beta$  are obtained. Reproduced from Atzmon, M. The pitalis of empirical thing of glass relaxation data with Saven brained an Reproduced from Atomorn Mathenpitallis of empirical fitting of glass relaxation data  $^{[45]}$  with stretched exponents. J. Appl. Phys. 2018, 123, 065103, with the permission of AIP Publishing [45].

# 8. Systematic Error in Spectrum Determination by Temperature Stepping [61]

One method of obtaining approximate spectra from relaxation measurements is based on measurements conducted by stepping the temperature from the lowest to the highest. It is then assumed that the behavior at each step i at temperature  $T_i$ , is dominated by a single activation free energy given by  $\Delta F_i = -k \frac{\partial ln\dot{\gamma}}{\partial (^1/_T)}\Big|_{T_i}$ . The assumption implicit in

Materials **2023**, 16, 0 13 of 23

# 8. Systematic Error in Spectrum Determination by Temperature Stepping [61]

One method of obtaining approximate spectra from relaxation measurements is based on measurements conducted by stepping the temperature from the lowest to the highest. It is then assumed that the behavior at each step i at temperature  $T_{i}$ , is dominated by a single activation free energy given by  $\Delta F_i = -k \frac{\partial ln\dot{\gamma}}{\partial (\frac{1}{T})}\Big|_{T_i}$ . The assumption implicit in this approximation is that at each step, processes with lower activation free energy have equilibrated, while those with higher activation free energy are frozen. Argon and Kuo [62] proposed this method to evaluate the activation free energy spectrum for torsional creep experiments. One aspect of the spectrum they obtained was a drop at the highest value of  $\Delta F_i$ . In contrast, Refs. [18,27] exhibit a monotonically increasing spectrum, which is also consistent with the free-volume model [27]. In this context, it is instructive to assess the error introduced by the approximation of a dominant activation free energy at each temperature step. For this purpose, we assumed a simple, monotonic, spectrum of activation free energies, qualitatively similar to that in Figure 5f. By simulating the process of anelastic relaxation at stepwise increasing temperatures, we obtained a simulated, apparent spectrum, based on the approximation of Ref. [62], which exhibits a decrease at the highest activation free energy (Figure 11). Comparison with the assumed input spectrum illustrates that the observed decrease is an artifact of the temperature-stepping method: processes with high activation energy are not completely frozen at lower temperatures, thus reducing

Materials 2023, 16, x FOR PEER REVINE's apparent contribution. Their participation at lower temperature also explains the strift to lower activation energies, seen in Figure 11.

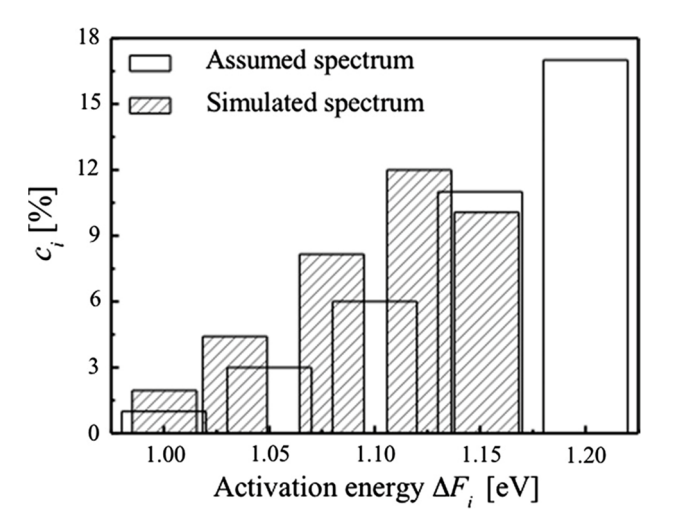


**Figure 11.** Assumed spectrum composer with the telectred from using the temperature strep strep approximation. Both the activation energy values and the spectrum is similar to those in Ref. [62]. Reprinted from Ju, J.D.: Atzmon, M. Evaluation of approximate measurements of activation-free-energy spectra of shear transformation zones in metallic measurements of activation-free-energy spectra of shear transformation zones in metallic glasses, J. Alloys Comp. **2015**, 643, S8–S10, Copyright (2014), with permission from Elsevier [61].

# 9. Characterization of Structural Evolution [63]

As mentioned in the introduction, glasses, until ke rysetallies onlid, untelegaconthing the vertical and interest and anti-ternal anni-librium state. Belowe these less is a single-interest, this extricts the price of the end of the condition of the price of the end of the e

Materials **2023**, 16, 0 14 of 23

initial stages of relaxation, where the latter is characterized by calorimetry. Efforts to design tough metallic glasses have included inducing the process opposite to structural relaxation, namely rejuvenation. This has been accomplished, e.g., by annealing above  $T_g$  [65] or by plastic deformation, including shot peening [66]. In addition, cyclic elastic loading [67], constrained loading [68] and irradiation [69,70] have led to rejuvenation. Cycling between room and cryogenic temperature has also been reported to lead to rejuvenation [71], as determined from measurements of stored enthalpy and yield. The authors proposed a rejuvenation mechanism due to heterogeneity of the thermal expansion coefficient, leading to microscopic stresses and local yielding. This novel result holds promise for practical applications, being non-destructive, controllable and isotropic [72–74]. It is noted, however, that, the authors have recently reported that the effect of cryogenic rejuvenation decays over time, likening the rejuvenation process to anelastic strain accumulation [75].

As with other examples, the lack of a periodic structure and microscopic structural probes poses challenges to obtaining a detailed description of the atomic-scale effect of cryogenic cycling. Relaxation-time spectra offer an opportunity for progress toward this goal. The nondestructive nature of cryogenic cycling offers an advantage in that the process preserves sample geometry. Two metallic glasses that undergo significant anelastic relaxation at room temperature, La<sub>70</sub>Cu<sub>15</sub>Al<sub>15</sub> and La<sub>70</sub>Ni<sub>15</sub>Al<sub>15</sub>, were investigated [63]. Figure 12 shows the anelastic strain as a function of time after constraining and releasing the samples following the same protocol as above. Curves were obtained for samples that

were allowed to age and structurally relax for several durations,  $1.9 \times 10^6$  to  $2.9 \times 10^7$  s, prior to constraining them. In one intermediate case, samples were also cycled between room and liquid-nitrogen temperature following the aging step. Not surprisingly, the amount of anelastic strain developed during the constraining period decreased with prior amount of anelastic strain developed during the constraining period decreased with prior room-temperature aging. For the as-prepared Law Luis-Alia alloy, the anelastic strain was nigher than higher than the clastic strain at the end of the constraining period. That the stress-free bigher than the clastic strain at the end of the constraining decreased with prior at the charge of the constraining decreased.

higher than the elastic strain at the end of the smeetraining period. That the stress-tree strainch was entirely anelastic avas refield by ennealing allower completes the bich are substained a complete second the original sample shape before it was constrained (See Figure 12).

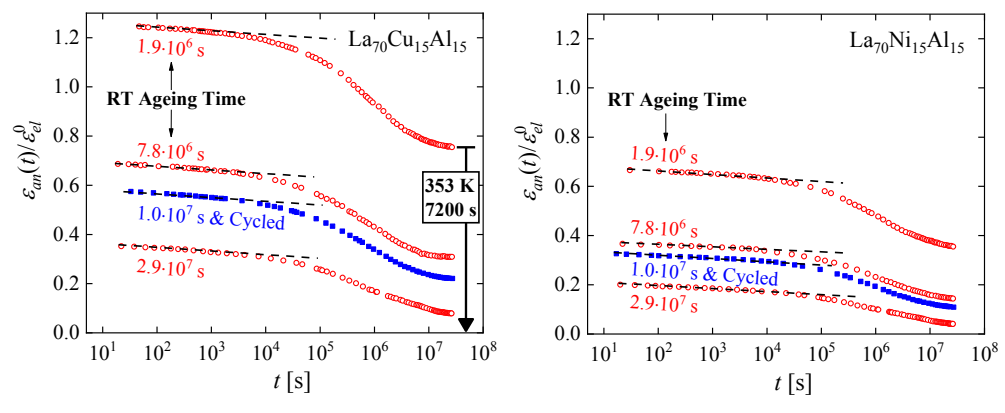


Figure 12. Normalized anelastic strain of Lazo Cu<sub>15</sub>Al<sub>15</sub> and Lazo Ni<sub>15</sub>Al<sub>15</sub> as a function of time for different aging times or printed the different aging times or time for different aging times or the different different aging times or the different differe

In the strain curves, there is no immediately obvious effect of cryogenic cycling. In the strain curve specthareois procedured the lightness of effect afration effect of cryogenic cycling. In the spectra (rightness characteristic constant) effect afration of the spectra (rightness constant) in the strain the lightness constant, and the constant constant of the cycles are not affected by cryogenic cycling: the areas under resolvable peaks or peak sets for the cycled samples fit on the same curve, as a function of aging time, as those for the aged samples that were not cycled (Figure 15). Based on the discussion in

Section 4, we conclude that structural relaxation associated with aging leads to a reduction in the number of *potential STZs*. The increase in time constants is likely due to an increase

Materials 2023, 16, 0 15 of 23

the corresponding time constants (Figure 14), restoring them to pre-aging values. However, the peak intensities are not affected by cryogenic cycling: the areas under resolvable peaks or peak sets for the cycled samples fit on the same curve, as a function of aging time, as those for the aged samples that were not cycled (Figure 15). Based on the discussion in Section 4, we conclude that structural relaxation associated with aging leads to a reduction in the number of *potential* STZs. The increase in time constants is likely due to an increase in the modulus of the glass, which increases the activation free energy for shear transformations (see present Equation (2) and Figure 7 in Ref. [76]). Cryogenic rejuvenation likely restores the elastic modulus. However, it does not lead to a recovery of the number density of *potential* STZs, as seen in the amount of normalized anelastic strain, is mainly on those consisting of a larger number of atoms, which are the slowest. This is seen qualitatively in Ref. [63], and

Materials 2023, 16, x FOR PEER REVIEW further detail for La<sub>55</sub>Ni<sub>20</sub>Al<sub>25</sub> in Figure 16 [76] which shows the evolution of 6each4  $c_m$  with aging time. The decrease of  $c_m$  with aging is likely a result of a decrease in free volume [12,27], as the density is known to increase with structural relaxation.

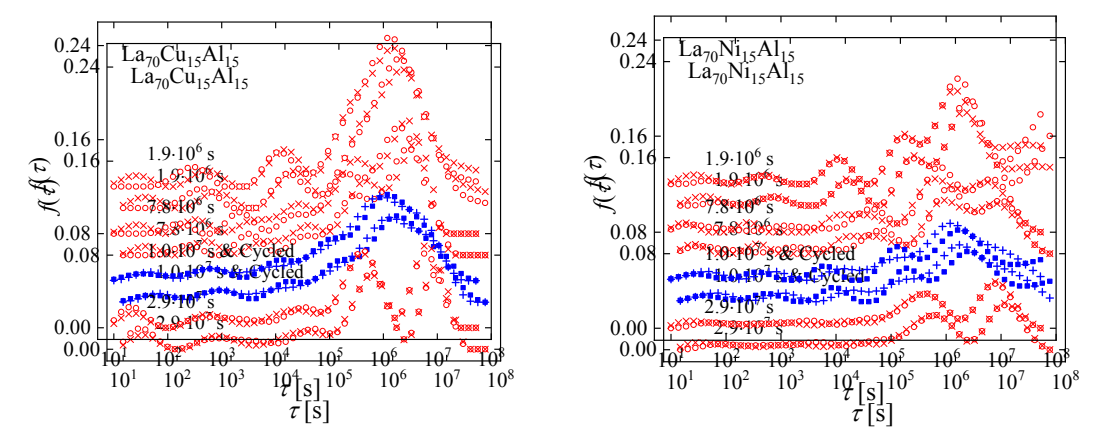


Figure 13. Relaxation-time spectra for Law Cuis Alis and Law Nins Alis with different aging times, as indicated for each condition? refresh that the last to two different samples are shown. Open an each condition? refresh that is the different samples are shown. Open an each condition of the samples are shown. Open an each condition of the samples without a supplier sample and shown. Open an each condition of the samples without Lei, T.J.; DaCosta, C.R.; Liu, M.; Wang, W.H.; Sun Y.H.; Greer, A.L.; M. Atzmon. Microscopic characterization of structural relaxation and cryogenic rejuvenation in metallic glasses. \*\*Months \*\*2019\*, 164, 165–170. \*\*Ethyland \*\*Condition\*\* \*\*2019\*, 164, 165–170. \*\*Ethyland \*\*2019\*, 165, 1765–170. \*\*Ethyland \*\*201

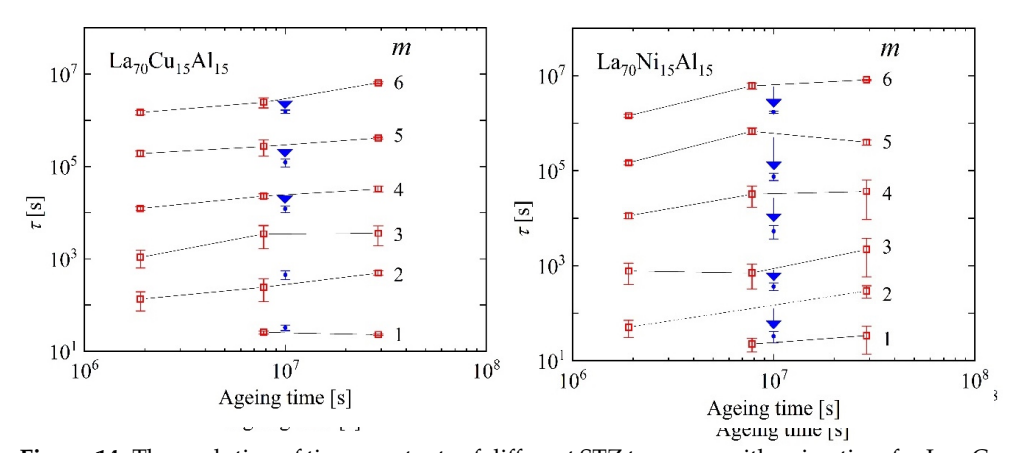


Figure 14: The evolution of time constants of different STZ types; "m, with resine time for Lew Cuts Alis after us. At I are all the constants of different STZ types; "m, with resine time for Lew Cuts Alis after us. At I are all types for the constants of different Lew Cuts and the cuts of the cuts and the cuts of th

Ageing time [s]

and La<sub>70</sub>Ni<sub>15</sub>Al<sub>15</sub> m ing aging. Reprin Materials **2023**, 16, 0 Atzmon. Microsco

**Figure 14.** The evolution of time constants of different STZ types, *m*, with aging time for La<sub>70</sub>Cu<sub>15</sub>Al<sub>15</sub> and La<sub>70</sub>Ni<sub>15</sub>Al<sub>15</sub> metallic glasses. Downwards arrows indicate the effect of cryogenic cycling following aging. Reprinted from Lei, T.J.; DaCosta, L.R.; Liu, M.; Wang, W.H.; Sun Y.H.; Greer, A.L.; M. Atzmon. Microscopic characterization of structural relaxation and cryogenic rejuvenation in metal-3 lic glasses. *Acta Mater.* **2019**, 164, 165–170. Copyright (2018), with permission from Elsevier [63].

Materials 2023, 16, x FOR PEER REVIEW

1.2

La<sub>70</sub>Cu<sub>15</sub>Al<sub>15</sub>

1.2

La<sub>70</sub>Ni<sub>15</sub>Al<sub>15</sub>

1.2

La<sub>70</sub>Ni<sub>1</sub>5Al<sub>15</sub> MGs. Blue: cycled after aging. Lihes: guide to the eye. Reprinted from Lei, T.J.; DaCosta, L.R.; Liu, M.; Wang, W.H.; Sun Y.H.; Greer, A.L.; M. Atzmon. Microscopic characterization of structural relaxation and cryogenic rejuvenation in metallic glasses. \*Acta Mater. 2019, 164, 165–170. Copyright (2018), with permission from Elsevier [63].

0.4

Using a wide range of experimental techniques, including x-ray photon spectroscopy. Gallino et al. [77] observed rapid relaxation, followed by quasi-stationary states in a Au-hased glass. The authors describe these states as reflecting structural relaxation pathways that are decompleted from the α relaxation, not involving demaification. In a related publication [78], it is shown that the vitrification kinetics upon cooling do not follow the Figure 15. co = the additive term in the spectrum fit, c<sub>5</sub> = the integrated area of the last two peaks, rights a line integrated area of the last two peaks, rights a line integrated area of the last two peaks, rights a line integrated area of the structural time integrated area of the structural place of the structural place of the structural place of the structural place. Some repetition and interpretation. The department of the structural relaxation and cryogenic refuvenation in metallic glasses. Acta Mater. 2019, 164, 165–170. billities of individual alloying elements.

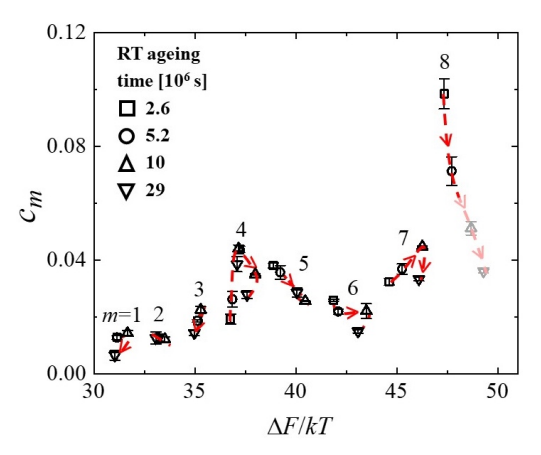


Figure 16. Volume fraction occupied by m-type potential STZs for Lass Nightle-potential requartion (6), as a function of of incidence exercises a figuration of the continuous forms of the continu

A few conclusions are noted here:

(1) Altion gricle genere refurencionate besotrieuro including a transported proved by the control of powerly by the control of the control of

laxation duction ging ethered results clearly show that the details are more nuanced. Generally, structural relaxation and rejuvenation cannot be described with a single variable.

Materials 2023, 16, 0 17 of 23

> (1) Although cryogenic rejuvenation does not restore the  $c_m$ , plasticity is improved by this process because of the increased fraction of potential STZ with a sufficiently short time constant to participate in deformation.

- A comparison of the time scale for *structural* relaxation,  $> 10^6$  s, with the shorter times for anelastic relaxation indicates that the mechanisms underlying the two processes cannot be assumed to be the same. The driving force for the former is thermodynamic, whereas for the latter it is mechanical.
- (3)While a measurement of a single variable, e.g., stored enthalpy or plasticity, may give the impression that the cryogenic cycling process leads to a reversal of structural relaxation due to aging, these results clearly show that the details are more nuanced. Generally, structural relaxation and rejuvenation cannot be described with a single variable.

Materials 2023, 16, x FOR PEER REVIEW

18 of 24

## 10. The Mechanism of the $\beta$ Relaxation [76]

Many glasses and glass types exhibit high-frequency secondary (β) relaxations in their Many glasses and glass types exhibit high-frequency secondary (β) relaxations in dynamic response [79–82]. These manifest in a second peak or a tail, e.g., in their loss modulus or dielectric susceptibility. For molecular glasses, the corresponding mechanisms modulus or dielectric susceptibility. For molecular glasses, the corresponding mechanisms modulus of dielectric susceptibility. For molecular glasses, the corresponding mechanisms modulus of dielectric susceptibility. can be straightforward—intermolecular ys. intramolecular relaxations. No such obvious distingtism is only known metallique grasses. Nevertheless/it has been guestes tidat bat β relaxations are due to a separate mechanism, further correlating it with plasticity and and sing speculations and in attentistic 1849; 1841; 1842; 1 bles been reported. 1851. Surexperimentalites alto and their and vais beaused to expluate this approach. In this section he actomic arale enechanism is discussed and the carrelation between a antigs enlantions and interticity with be avaluated in the next section.

Equipped with a anegwine or too do logger of any living encertainise laxelax ations, I we studied the STZ-spectra of Laar Niad Alasnemuta Hiaglasurvith aircuiticant laxalaxation. [76]. A plot of the STZ valume,  $M_{masia}$  a function of n, r is figure 1, the vertex of the ging impse. The atomic volumeabhaineachformthealdprésis 1.1461 x 129 Th<sup>s</sup> for foratmald and fiezs Taze, and 0.236×10.0° ni<sup>s</sup> not language alock STXsSAZ befAre before; allgets time of the line entended to the line. Tibren formakrevial closis to lobset tof thrat Abatam, AD. 1466m, 10-176663 xw110-1768 srther easy tible in latter abovuit lh2% albohut i12%n afcthric melumatofulue albhur Sienulathre alltsy. w Siln til ar sle suelte givriet, two stopeoleginned, inverse Cosenhedrich Landing 1864 NVIII by in ing Abe 4064 ultivitätet akay be bbesa dlatprevidutak littirelly slopy suggest libertaliffetteer sleggest tiplay differeint fektimerals play a Folesin fast vs. slow STZs.

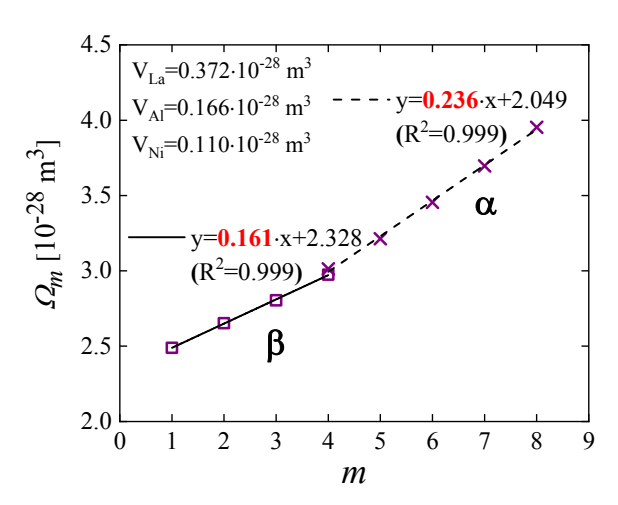


Figure 47. SEZ-SNY4M1 $\Omega$  OFE a blunction STZ-by return thors STE by reconstruction set  $10^7~{
m s}$ . The error bars, <0.4%, are smaller than the symbols. The stopes correspond to the volume increment between two ment The error bars; \*0.7%; are smaller than the symbols. The slopes correspond to the volume inclement adjacent \( \int\_{m} \) values. The random error in these slopes is 2–3%. Reproduced from Lei, T.J.; Liu, M.; between two adjacent \( \int\_{m} \) values. The random error in these slopes is 2–3%. Reproduced from Lei, Wang, W.H.; Sun, Y.H.; Greer, A.L.; Atzmon, M. Shear transformation zone analysis of anelastic T.J.; Liu, M.; Wang, W.H.; Greer, A.L.; Atzmon, M. Shear transformations: This is of relaxation of a metallic glass reveals distinct properties of \( \alpha \) and \( \beta \) refaxations. This is of the same transformation of the  $\alpha$  and  $\beta$  relaxation of a metallic glass reveals distinct properties of  $\alpha$  and  $\beta$  relaxations. Phys Rev. E 2019, 100, 033001 [76].

In Refs. [18,76,86], a single mechanism, namely shear transformations, consistently describes the entire range of relaxation times observed. This suggests that even though the  $\beta$  relaxation appears distinct in the loss modulus for some metallic glasses, a separate mechanism need not be invoked. This is seen when  $E''(\omega)$  is computed [44] from the exmontal spectrum obtained for quasi-static relayation [18]—it aybibits a bigh-fro

Materials **2023**, 16, 0 18 of 23

11. STZ Properties and Plasticity [86]

In Refs. [18,76,86], a single mechanism, namely shear transformations, consistently describes the entire range of relaxation times observed. This suggests that even though the  $\beta$  relaxation appears distinct in the loss modulus for some metallic glasses, a separate mechanism need not be invoked. This is seen when  $E''(\omega)$  is computed [44] from the experimental spectrum obtained for quasi-static relaxation [18] – it exhibits a high-frequency tail (Figure 9b) despite the fact that the spectrum corresponds to a single mechanism.

In much of the literature, e.g., Refs. [87,88], the  $\alpha$  and  $\beta$  relaxations are discussed in

terms of their reversibility vs. irreversibility. The  $\alpha$  relaxation, generally associated with the glass transition, is described as irreversible whereas the  $\beta$  relaxation is described as reversible. Ref. [89] goes further and suggests that some  $\beta$  relaxations are reversible, and others are not. We argue that reversibility or lack thereof are not inherent properties of these relaxations. As mentioned above, STZs are reversible when their volume fraction is small, but become irreversible at high volume fraction as a result of loss of back-stress. Our anelastic relaxation experiments demonstrate that all STZ sizes, including those underlying both the  $\alpha$  and  $\beta$  relaxation are reversible at high volume fraction as a result of loss of back-stress. volume fraction are all strains when they occupy a small volume fraction are a result of loss of back-stress.

As mentioned above, it has been suggested that the β relaxation is responsible for alloy plasticity [STZ-Proper 6584 Plasticity 1876] specially above this assertion was the similarity in activation energy for plasticity and the Barcharations extend of politicity represents the Barcharations extend this assertion was the similarity in Despite their similar compositions at the horizon of plasticity presents itself in the Assertion of Plasticity presents itself in the Assertion of Plasticity presents itself in the Assertion of Plasticity presents itself in the Same methodology and Layout Alis. The same methodology the susual as in the cases above to determine the SIZ spectra, followed by the same methodology the tensile behavior of Plasticity presents itself in the SIZ spectra, followed by the same methodology the tensile behavior of Plasticity and Layout Island to the cases above to determine the SIZ spectra, followed by the same methodology the tensile behavior of Plasticity and Layout Island Plasticity of Size of the SIZ spectra, followed by the same methodology the tensile behavior of Plasticity and Plasticity Island Plasticity of Size of the Size of the Size of Size of

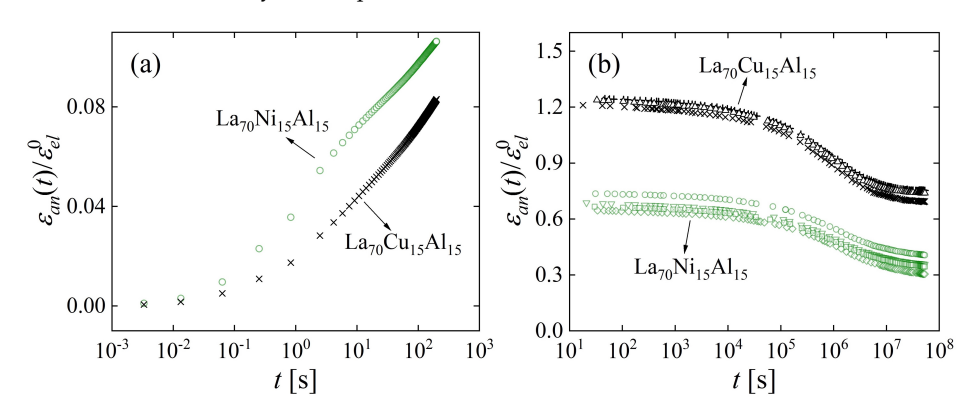
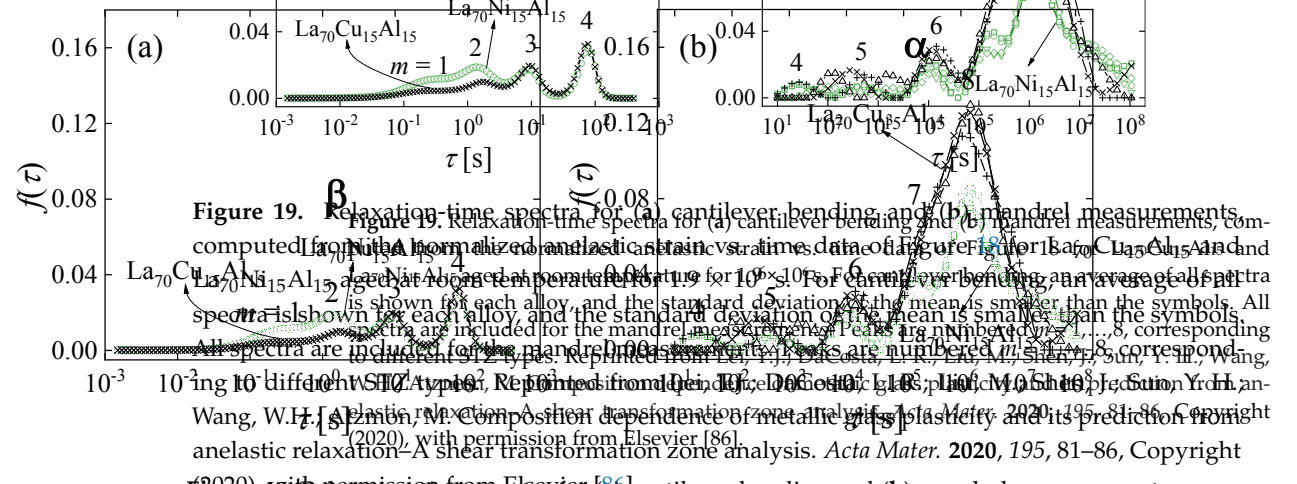


Figure 18. Ane lastic strain, normalized by the corresponding souilibrium plastic strain strain, we for for (a) cantilever bending and the construction of the continued by the corresponding souilibrium prior prior room-temperature trainers from \$100 \times 100 \ti

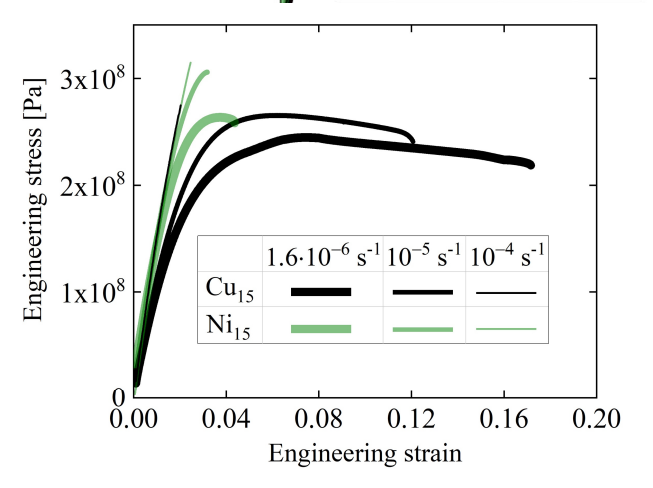
×  $10^{-6}$  s<sup>-1</sup> to  $10^{-4}$  s<sup>-1</sup> (Figure 20). At the two lower rates, La<sub>20</sub>Cu<sub>15</sub>Al<sub>15</sub> exhibited far greater plasticity, with up to > 17% engineering strain. It is noted that this example shows a negative correlation of  $\beta$  intensity with plasticity, the opposite of that proposed in Ref. [83]. While 17% engineering strain is beyond the linear regime of non-interacting STZs, the STZ spectra can be used to qualitatively explain the difference in mechanical behavior between

the observed room-temperature tensile deformation. We propose that the deformation cannot be accounted for biethe 20 deep and represent an activated \$12.5 tolers with the deformation as the first that the state of the first state of the firs



regard 19! the exemission from the perfect strain vs. time data of Figure 18 for Law Cuis Alis and Law Nil Anitage in 18 the two relayers to the the two relayers to the perfect of it shows for each only, and the granters of the perfect of the per

20



LawCu15Al15 and LawNi15Al15 obtained from  $10^{-6}$  s<sup>-1</sup>,  $10^{-5}$  s<sup>-1</sup>, and  $10^{-4}$  s<sup>-1</sup>. Curve thickness sts of 200–20,000 data points, depending on 1en, J.; Sun, Y. H.; Wang, W.H.; Atzmon, M.

Figure 20. Engineering stress vs. engineering strain for La<sub>20</sub>Cu<sub>15</sub>Al<sub>15</sub> and La<sub>20</sub>Ni<sub>15</sub>Al<sub>15</sub> obtained figure 20. Engineering stress vs. engineering strain for La<sub>20</sub>Cu<sub>15</sub>Al<sub>15</sub> and La<sub>20</sub>Ni<sub>15</sub>Al<sub>15</sub> obtained from room-room-representation the strain strains of the solution of th

For the stress applied in the tensile measurements, the strain rate obtained is higher than that expected from the active STZs observed. Similarly, the total strain in Figure 20 cannot be accounted for by the total volume fraction of active STZs contributing to Figures 17 and 18. This

Materials 2023, 16, 0 20 of 23

is likely a result of STZ interactions due to their high concentration at these strain values, leading to a reduction in their elastic energy barrier and therefore enhanced kinetics [19]. Thus, larger STZs than those participating in linear anelasticity contribute to the observed room-temperature tensile deformation. We propose that the deformation observed in Figure 20 does not represent an activated flow state, such as described in Ref. [12], for which a steady-state structure is achieved by repeated regeneration. Rather, we argue, this deformation is in a transient state, which persists as long as *potential* STZs keep up with the applied strain. Beyond this point, the increasing applied strain is accommodated by localization, resulting in failure. Since the  $La_{70}Cu_{15}Al_{15}$  alloy contains an *overall* higher volume fraction occupied by *potential* STZs than  $La_{70}Ni_{15}Al_{15}$  does, the former reaches higher strains before it fails.

# 12. Additional Properties

There may be potential for expanding the STZ model to describe additional atomic transport phenomena not addressed in this review. Argon and Shi [19] address the limit of the model, when back-stress is lost due to STZs being in close proximity to each other. Short-range diffusion, e.g., in multilayered thin films with short modulation wavelength, could take place by small displacements associated with STZs. This would be consistent with the observation of two different time constants for interdiffusion in modulated Ni-Zr thin films [91]. Flow or long-range diffusion would require STZ percolation. For flow to take place, the volume fraction that is rigid, i.e., does *not* contain active *potential* STZs,  $\exp(-\sum_{n=1}^{n_0} c_n)$ , where  $n_0$  is the temperature-dependent maximum size of such *potential* STZs, has to be *below* the percolation threshold. Otherwise, the matrix is rigid. The requirement for long-range diffusion is less strict:  $1 - \exp(-\sum_{n=1}^{n_0} c_n)$ , the volume fraction occupied by active *potential* STZs, has to exceed the percolation threshold. As noted above, overlapping *potential* STZs are counted multiple times, so  $\sum_{n=1}^{n_0} c_n > 1$  is possible [27].

# 13. Conclusions

Due to the lack of periodicity, microscopic atomic rearrangements in metallic glasses can typically only be inferred indirectly from experiment. While physical analogs and molecular dynamics have contributed important insights, they are not suitable for simulating processes with a wide range of activation free energy and therefore time constants. We show here that anelastic relaxation, conducted over a wide range of time constants, can provide important insights when combined with spectrum determination. This work will hopefully motivate further simulations and experiments. For example, since the number of directions in phase space is too large to comprehensively capture in atomistic simulations, the present results could offer possible directions to probe in order to determine the barriers to possible shear transformations, e.g., by extending Ref. [92]. Atom-probe tomography investigations of chemical heterogeneity could help evaluate the conclusions that suggest composition differences between fast and slow STZs.

**Funding:** This research was funded by the U.S. National Science Foundation (NSF), Grants Nos. DMR-1307884 and DMR-1708043.

**Data Availability Statement:** No new data were created or analyzed in this study. Data sharing is not applicable to this article.

**Acknowledgments:** Contributions to the research reviewed in this publication were made by L. R. DaCosta, A. L. Greer, D. Jang, M. Liu, A. Nwankpa, J. Shen, Y. H. Sun and W. H. Wang. We thank Frans Spaepen for useful discussions.

Materials **2023**, 16, 0 21 of 23

**Conflicts of Interest:** Author Jong Doo Ju is employed by Ford Motor Company. The remaining authors declare that the research was conducted in the absence of any commercial or financial relationships that could be construed as a potential conflict of interest. The funders had no role in the design of the study; in the collection, analyses, or interpretation of data; in the writing of the manuscript; or in the decision to publish the results.

#### References

- 1. Buckel, W.; Hilsch, R. Einfluß der Kondensation bei tiefen Temperaturen auf den elektrischen Widerstand und die Supraleitung für verschiedene Metalle. Z. Phys. 1954, 138, 109–120. [CrossRef]
- 2. Klement, W.; Willens, R.H.; Duwez, P.O. Non-crystalline structure in solidified gold–silicon alloys. *Nature* 1960, 187, 869–870. [CrossRef]
- 3. Drehman, A.J.; Greer, A.L. Kinetics of crystal nucleation and growth in Pd<sub>40</sub>Ni<sub>40</sub>P<sub>20</sub> glass. *Acta Metall.* 1984, 32, 323–332. [CrossRef]
- 4. Inoue, A.; Zhang, T.; Masumoto, T. Production of amorphous cylinder and sheet of La<sub>55</sub>Al<sub>25</sub>Ni<sub>20</sub> alloy by a metallic mold casting method. *Mater. Trans. JIM* **1990**, *31*, 425–4288. [CrossRef]
- Peker, A.; Johnson, W.L. A highly processable metallic glass: Zr<sub>41.2</sub>Ti<sub>13.8</sub>Cu<sub>12.5</sub>Ni<sub>10.0</sub>Be<sub>22.5</sub>. Appl. Phys. Lett. 1993, 63, 2342–2344. [CrossRef]
- 6. Ashby, M.F.; Greer, A.L. Metallic glasses as structural materials. Scr. Mater. 2006, 54, 321–326. [CrossRef]
- 7. Schroers, J.; Nguyen, T.; O'Keeffe, S.; Desai, A. Thermoplastic forming of bulk metallic glass—Applications for MEMS and microstructure fabrication. *Mater. Sci. Eng. A* **2007**, 449, 898–902. [CrossRef]
- 8. Hull, D.; Bacon, D.J. Introduction to Dislocations, 5th ed.; Elsevier: Amsterdam, The Netherlands, 2011.
- 9. Bragg, W.L.; Nye, J.F. A dynamical model of a crystal structure. Proc. R. Soc. Lond. Ser. A Math. Phys. Sci. 1947, 190, 474–481.
- 10. Hirsch, P.; Cockayne, D.; Spence, J.; Whelan, M. 50 Years of TEM of dislocations: Past, present and future. *Philos. Mag.* **2006**, 86, 4519–4528. [CrossRef]
- 11. Orowan, E. Creep in metallic and nonmetallic materials. In Proceedings of the First U.S. National Congress of Applied Mechanics: Held at Illinois Institute of Technology, Chicago, IL, USA, 11–16 June 1951; pp. 453–472.
- 12. Argon, A.S. Plastic deformation in metallic glasses. Acta Metall. 1979, 27, 47–58. [CrossRef]
- 13. Harmon, J.S.; Demetriou, M.D.; Johnson, W.L.; Samwer, K. Anelastic to plastic transition in metallic glass-forming liquids. *Phys. Rev. Lett.* **2007**, *99*, 135502. [CrossRef] [PubMed]
- 14. Demetriou, M.D.; Johnson, W.L.; Samwer, K. Coarse-grained description of localized inelastic deformation in amorphous metals. *Appl. Phys. Lett.* **2009**, *94*, 191905. [CrossRef]
- 15. Argon, A.S.; Kuo, H.Y. Plastic flow in a disordered bubble raft (an analog of a metallic glass). Mater. Sci. Eng. 1979, 39, 101–109. [CrossRef]
- 16. Schall, P.; Weitz, D.A.; Spaepen, F. Structural rearrangements that govern flow in colloidal glasses. *Science* **2007**, *318*, 1895–1899. [CrossRef] [PubMed]
- 17. Falk, M.L.; Langer, J.S. Dynamics of viscoplastic deformation in amorphous solids. Phys. Rev. E 1998, 57, 7192–7205. [CrossRef]
- 18. Ju, J.D.; Jang, D.; Nwankpa, A.; Atzmon, M. An atomically quantized hierarchy of shear transformation zones in a metallic glass. *J. Appl. Phys.* **2011**, *109*, 053522. [CrossRef]
- 19. Argon, A.S.; Shi, L.T. Development of visco-plastic deformation in metallic glasses. Acta Metall. 1983, 31, 499–507. [CrossRef]
- 20. Liu, S.T.; Wang, Z.; Peng, H.L.; Yu, H.B.; Wang, W.H. The activation energy and volume of flow units of metallic glasses. *Scr. Mater.* **2012**, *67*, 9–12. [CrossRef]
- Kato, H.; Igarashi, H.; Inoue, A. Another clue to understand the yield phenomenon at the glassy state in Zr<sub>55</sub>Al<sub>10</sub>Ni5Cu<sub>30</sub> metallic glass. *Mater. Lett.* 2008, 62, 1592–1594.
- 22. Cost, J.R. Nonlinear regression least-squares method for determining relaxation time spectra for processes with first-order kinetics. *J. Appl. Phys.* **1983**, *54*, 2137–2146. [CrossRef]
- 23. Available online: http://s-provencher.com/contin.shtml (accessed on 14 November 2023).
- 24. Provencher, S.W. A constrained regularization method for inverting data represented by linear algebraic or integral equations. *Comput. Phys. Commun.* **1982**, 27, 213–227. [CrossRef]
- 25. Provencher, S.W. CONTIN: A general purpose constrained regularization program for inverting noisy linear algebraic and integral equations. *Comput. Phys. Commun.* **1982**, 27, 229–242. [CrossRef]
- 26. Lakes, R.S. Viscoelastic Solids; CRC Press: Boca Baton, FL, USA, 1999.
- 27. Atzmon, M.; Ju, J.D. Microscopic description of flow defects and relaxation in metallic glasses. *Phys. Rev. E* **2014**, *90*, 042313. [CrossRef] [PubMed]
- 28. Lei, T.J.; Atzmon, M. Activation volume details from nonlinear anelastic deformation of a metallic glass. *J. Appl. Phys.* **2019**, 126, 185104. [CrossRef]
- 29. Delogu, F. Identification and characterization of potential shear transformation zones in metallic glasses F. *Phys. Rev. Lett.* **2008**, 100, 255901. [CrossRef] [PubMed]
- 30. Neudecker, M.; Mayr, S.G. Dynamics of shear localization and stress relaxation in amorphous Cu<sub>50</sub>Ti<sub>50</sub>. *Acta Mater.* **2009**, 57, 1437–1441. [CrossRef]
- 31. Johnson, W.L.; Samwer, K. A universal criterion for plastic yielding of metallic glasses with a  $(T/T_g)^{2/3}$  temperature dependence. *Phys. Rev. Lett.* **2005**, 95, 195501. [CrossRef]
- 32. Pan, D.; Inoue, A.; Sakurai, T.; Chen, M.W. Experimental characterization of shear transformation zones for plastic flow of bulk metallic glasses. *Proc. Nat. Acad. Sci. USA* **2008**, *105*, 14769. [CrossRef]

Materials **2023**, 16, 0 22 of 23

33. Krausser, J.; Samwer, K.; Zaccone, A. Interatomic repulsion softness directly controls the fragility of supercooled metallic melts. *Proc. Natl. Acad. Sci. USA* **2015**, *112*, 13762. [CrossRef]

- 34. Ju, J.D.; Atzmon, M. A comprehensive atomistic analysis of the experimental dynamic-mechanical response of a metallic glass. *Acta Mater.* **2014**, 74, 183–188. [CrossRef]
- 35. Pelletier, J.M. Dynamic mechanical properties in a Zr<sub>46.8</sub>Ti<sub>13.8</sub>Cu<sub>12.5</sub> Ni<sub>10</sub>Be<sub>27.5</sub> bulk metallic glass. *J. Alloys Compd.* **2005**, 393, 223–230. [CrossRef]
- 36. Keryvin, V.; Vaillant, M.-L.; Rouxel, T.; Huger, M.; Gloriant, T.; Kawamura, Y. Thermal stability and crystallisation of a Zr<sub>55</sub>Cu<sub>30</sub>Al<sub>10</sub>Ni<sub>5</sub> bulk metallic glass studied by in situ ultrasonic echography. *Intermetallics* **2002**, *10*, 1289–1296. [CrossRef]
- 37. Rouxel, T. Elastic properties and short-to medium-range order in glasses. J. Am. Ceram. Soc. 2007, 90, 3019–3039. [CrossRef]
- 38. Wang, J.Q.; Wang, W.H.; Bai, H.Y. Extended elastic model for flow in metallic glasses. J. Non-Cryst. Solids 2011, 357, 223–226. [CrossRef]
- 39. Wang, W.H. The elastic properties, elastic models and elastic perspectives of metallic glasses. Prog. Mater. Sci. 2012, 57, 487–656. [CrossRef]
- 40. Ngai, K.L.; Plazek, D.J.; Rendell, R.W. Some examples of possible descriptions of dynamic properties of polymers by means of the coupling model. *Rheol. Acta* **1997**, *36*, 307–319. [CrossRef]
- 41. Salmén, L. Viscoelastic properties of in situ lignin under water-saturated conditions. J. Mater. Sci. 1984, 19, 3090–3096. [CrossRef]
- 42. Qiao, J.C.; Pelletier, J.M. Mechanical relaxation in a Zr-based bulk metallic glass: Analysis based on physical models. *J. Appl. Phys.* **2012**, *112*, 033518. [CrossRef]
- 43. Jeong, H.T.; Fleury, E.; Kim, W.T.; Kim, D.H.; Hono, K. Study on the mechanical relaxations of a Zr<sub>36</sub>Ti<sub>24</sub>Be<sub>40</sub> amorphous alloy by time–temperature superposition principle. *J. Phys. Soc. Jpn.* **2004**, *11*, 3192. [CrossRef]
- 44. Ju, J.D.; Atzmon, M. Atomistic interpretation of the dynamic response of glasses. MRS Comm. 2014, 4, 63–66. [CrossRef]
- 45. Atzmon, M. The pitfalls of empirical fitting of glass relaxation data with stretched exponents. J. Appl. Phys. 2018, 123, 065103. [CrossRef]
- 46. Kohlrausch, V.R. Theory of the electric residue in the Leyden jar. Ann. Phys. Chem. (Poggendorff) 1854, 91, 179–214. [CrossRef]
- 47. Williams, G.; Watts, D.C. Non-symmetrical dielectric relaxation behaviour arising from a simple empirical decay function. *Trans. Faraday Soc.* **1970**, *66*, 80–85. [CrossRef]
- 48. Williams, G.; Watts, D.; Dev, S.B.; North, A.M. Further considerations of non symmetrical dielectric relaxation behaviour arising from a simple empirical decay function. *Trans. Faraday Soc.* **1971**, *67*, 1323–1335. [CrossRef]
- 49. Phillips, J.C. Stretched exponential relaxation in molecular and electronic glasses. Rep. Prog. Phys. 1996, 59, 1133. [CrossRef]
- 50. MacDonald, J.R. Linear relaxation: Distributions, thermal activation, structure, and ambiguity. J. Appl. Phys. 1987, 62, R51–R62. [CrossRef]
- 51. Svare, I.; Martin, S.W.; Borsa, F. Stretched exponentials with *T*-dependent exponents from fixed distributions of energy barriers for relaxation times in fast-ion conductors. *Phys. Rev. B* **2000**, *61*, 228–233. [CrossRef]
- 52. Hodge, I.M. Enthalpy relaxation and recovery in amorphous materials. *J. Non-Cryst. Solids* **1994**, *169*, 211–266, and references therein. [CrossRef]
- 53. Qiao, J.C.; Pelletier, J.M. Enthalpy relaxation in Cu<sub>46</sub>Zr<sub>45</sub>Al<sub>7</sub>Y<sub>2</sub> and Zr<sub>55</sub>Cu<sub>30</sub>Ni<sub>5</sub>Al<sub>10</sub> bulk metallic glasses by differential scanning calorimetry (DSC). *Intermetallics* **2011**, *19*, 9–18. [CrossRef]
- 54. Raghavan, R.; Murali, P.; Ramamurty, U. Influence of cooling rate on the enthalpy relaxation and fragility of a metallic glass. *Metall. Mater. Trans. A* **2008**, *39*, 1573–1577. [CrossRef]
- 55. Kawai, K.; Hagiwara, T.; Takai, R.; Suzuki, T. Comparative investigation by two analytical approaches of enthalpy relaxation for glassy glucose, sucrose, maltose, and trehalose. *Pharm. Res.* **2005**, 22, 490–495, and references therein. [CrossRef] [PubMed]
- 56. Hu, L.; Yue, Y. Secondary relaxation in metallic glass formers: Its correlation with the genuine Johari Goldstein relaxation. *J. Phys. Chem. C.* **2009**, *113*, 15001–15006. [CrossRef]
- 57. Qiao, J.C.; Casalini, R.; Pelletier, J.M. Main (α) relaxation and excess wing in Zr50Cu40Al10 bulk metallic glass investigated by mechanical spectroscopy. *J. Non-Cryst. Solids* **2015**, 407, 106–109. [CrossRef]
- 58. Zhao, Z.F.; Wen, P.; Shek, C.H.; Wang, W.H. Measurements of slow β-relaxations in metallic glasses and supercooled liquids. *Phys. Rev. B* **2007**, *75*, 174201. [CrossRef]
- 59. Rösner, P.; Samwer, K.; Lunkenheimer, P. Indications for an "excess wing" in metallic glasses from the mechanical loss modulus in Zr<sub>65</sub>Al<sub>7.5</sub>Cu<sub>27.5</sub>. *Europhys. Lett.* **2004**, *68*, 226. [CrossRef]
- 60. Brand, R.; Lunkenheimer, P.; Schneider, U.; Loidl, A. Is there an excess wing in the dielectric loss of plastic crystals? *Phys. Rev. Lett.* **1999**, 82, 1951. [CrossRef]
- 61. Ju, J.D.; Atzmon, M. Evaluation of approximate measurements of activation-free-energy spectra of shear transformation zones in metallic glasses. *J. Alloys Comp.* **2015**, *643*, S8–S10. [CrossRef]
- 62. Argon, A.S.; Kuo, H.Y. Free energy spectra for inelastic deformation of five metallic glass alloys. *J. Non-Cryst. Solids* **1980**, 37, 241–266. [CrossRef]
- 63. Lei, T.J.; DaCosta, L.R.; Liu, M.; Wang, W.H.; Sun, Y.H.; Greer, A.L.; Atzmon, M. Microscopic characterization of structural relaxation and cryogenic rejuvenation in metallic glasses. *Acta Mater.* **2019**, *164*, 165–170. [CrossRef]
- 64. Zhao, J.; Gao, M.; Ma, M.; Cao, X.; He, Y.; Wang, W.; Luo, J. Influence of annealing on the tribological properties of Zr-based bulk metallic glass. *J. Non-Cryst. Solids* **2018**, 481, 94–97. [CrossRef]
- 65. Kumar, G.; Rector, D.; Conner, R.D.; Schroers, J. Embrittlement of Zr-based bulk metallic glasses. Acta Mater. 2009, 57, 3572–3583. [CrossRef]
- 66. Concustell, A.; Méar, F.O.; Surinach, S.; Baró, M.D.; Greer, A.L. Structural relaxation and rejuvenation in a metallic glass induced by shot-peening. *Phil. Mag. Lett.* **2009**, *89*, 831. [CrossRef]

Materials **2023**, 16, 0 23 of 23

67. Louzguine-Luzgin, D.V.; Zadorozhnyy, V.Y.; Ketov, S.V.; Wang, Z.; Tsarkov, A.A.; Greer, A.L. On room-temperature quasi-elastic mechanical behaviour of bulk metallic glasses. *Acta Mater.* **2017**, *129*, 343–351. [CrossRef]

- 68. Pan, J.; Wang, Y.X.; Guo, Q.; Zhang, D.; Greer, A.L.; Li, Y. Extreme rejuvenation and softening in a bulk metallic glass. *Nat. Commun.* **2018**, *9*, 560. [CrossRef] [PubMed]
- 69. Magagnosc, D.J.; Kumar, G.; Schroers, J.; Felfer, P.; Cairney, J.M.; Gianola, D.S. Effect of ion irradiation on tensile ductility, strength and fictive temperature in metallic glass nanowires. *Acta Mater.* **2014**, *74*, 165–182. [CrossRef]
- 70. Heo, J.; Kim, S.; Ryu, S.; Jang, D. Delocalized Plastic Flow in Proton-Irradiated Monolithic Metallic Glasses. *Sci. Rep.* **2016**, 6, 23244. [CrossRef]
- 71. Ketov, S.V.; Sun, Y.H.; Nachum, S.; Lu, Z.; Checchi, A.; Beraldin, A.R.; Bai, H.Y.; Wang, W.H.; Louzguine-Luzgin, D.V.; Carpenter, M.A.; et al. Rejuvenation of metallic glasses by non-affine thermal strain. *Nature* **2015**, *524*, 200–203. [CrossRef]
- 72. Miyazaki, N.; Wakeda, M.; Wang, Y.-J.; Ogata, S. Prediction of pressure-promoted thermal rejuvenation in metallic glasses. *npj Comput. Mater.* **2016**, 2, 1–9. [CrossRef]
- 73. Madge, S.V.; Louzguine-Luzgin, D.V.; Kawashima, A.; Greer, A.L.; Inoue, A. Compressive plasticity of a La-based glass-crystal composite at cryogenic temperatures. *Mater. Des.* **2016**, *101*, 146–151. [CrossRef]
- 74. Grell, D.; Dabrock, F.; Kerscher, E. Cyclic cryogenic pretreatments influencing the mechanical properties of a bulk glassy Zr-based alloy. *Fatigue Fract. Eng. Mater. Struct.* **2018**, *41*, 1330–1343. [CrossRef]
- 75. Costa, M.B.; Londoño, J.J.; Blatter, A.; Hariharan, A.; Gebert, A.; Carpenter, M.A.; Greer, A.L. Anelastic-like nature of the rejuvenation of metallic glasses by cryogenic thermal cycling. *Acta Mater.* **2023**, 244, 118551. [CrossRef]
- 76. Lei, T.J.; Liu, M.; Wang, W.H.; Sun, Y.H.; Greer, A.L.; Atzmon, M. Shear transformation zone analysis of anelastic relaxation of a metallic glass reveals distinct properties of α and β relaxations. *Phys. Rev. E* **2019**, *100*, 033001. [CrossRef]
- 77. Gallino, I.; Cangialosi, D.; Evenson, Z.; Schmitt, L.; Hechler, S.; Stolpe, M.; Beatrice Ruta, B. Hierarchical aging pathways and reversible fragile-to-strong transition upon annealing of a metallic glass former. *Acta Mater.* **2018**, *144*, 400–410. [CrossRef]
- 78. Monnier, X.; Cangialosi, D.; Ruta, B.; Busch, R.; Gallino, I. Vitrification decoupling from α-relaxation in a metallic glass. *Sci. Adv.* **2020**, *6*, eaay1454. [CrossRef] [PubMed]
- 79. Johari, G.P.; Goldstein, M. Molecular mobility in simple glasses. J. Phys. Chem. 1970, 74, 2034–2035. [CrossRef]
- 80. Schneider, U.; Brand, R.; Lunkenheimer, P.; Loidl, A. Excess wing in the dielectric loss of glass formers: A Johari-Goldstein β relaxation? *Phys. Rev. Lett.* **2000**, *84*, 5560. [CrossRef]
- 81. Cohen, Y.; Karmakar, S.; Procaccia, I.; Samwer, K. The nature of the β-peak in the loss modulus of amorphous solids. *Europhys. Lett.* **2012**, *100*, 36003. [CrossRef]
- 82. Johari, G.P.; Goldstein, M. Viscous liquids and the glass transition. II. Secondary relaxations in glasses of rigid molecules. *J. Chem. Phys.* **1970**, 53, 2372–2388. [CrossRef]
- 83. Yu, H.B.; Shen, X.; Wang, Z.; Gu, L.; Wang, W.H.; Bai, H.Y. Tensile Plasticity in Metallic Glasses with Pronounced β relaxations. *Phys. Rev. Lett.* **2012**, *108*, 015504. [CrossRef]
- 84. Yu, H.B.; Wang, W.H.; Bai, H.Y.; Wu, Y.; Chen, M.W. Relating activation of shear transformation zones to β relaxations in metallic glasses. *Phys. Rev. B* **2010**, *81*, 220201. [CrossRef]
- 85. Küchemann, S.; Maaß, R. Gamma relaxation in bulk metallic glasses. Scr. Mater. 2017, 137, 5–8. [CrossRef]
- 86. Lei, T.J.; DaCosta, L.R.; Liu, M.; Shen, J.; Sun, Y.H.; Wang, W.H.; Atzmon, M. Composition dependence of metallic glass plasticity and its prediction from anelastic relaxation—A shear transformation zone analysis. *Acta Mater.* **2020**, *195*, 81–86. [CrossRef]
- 87. Qiao, J.C.; Pelletier, J.M. Dynamic Mechanical Relaxation in Bulk Metallic Glasses: A Review. J. Mater. Sci. Tech. 2014, 30, 523–545. [CrossRef]
- 88. Hao, Q.; Pineda, E.; Wang, Y.-J.; Yang, Y.; Qiao, J.C. Reversible anelastic deformation mediated by β relaxation and resulting two-step deformation in a La<sub>60</sub>Ni<sub>15</sub>Al<sub>25</sub> metallic glass. *Phys. Rev. B* **2023**, *108*, 024101. [CrossRef]
- 89. Zhao, R.; Jiang, H.Y.; Luo, P.; Shen, L.Q.; Wen, P.; Sun, Y.H.; Bai, H.Y.; Wang, W.H. Reversible and irreversible β-relaxations in metallic glasses. *Phys. Rev. B* **2020**, *101*, 094203. [CrossRef]
- 90. Wang, X.D.; Ruta, B.; Xiong, L.H.; Zhang, D.W.; Chushkin, Y.; Sheng, H.W.; Lou, H.B.; Cao, Q.P.; Jiang, J.Z. Free-volume dependent atomic dynamics in beta relaxation pronounced La-based metallic glasses. *Acta Mater.* **2015**, *99*, 290–296. [CrossRef]
- 91. Atzmon, M.; Spaepen, F. Study of Interdiffusion in Amorphous Compositionally Modulated Ni-Zr Thin Films. In *Science and Technology of Rapidly Quenched Alloys*; Tenhover, M., Johnson, W.L., Tanner, L.E., Eds.; Materials Research Society: Pittsburgh, PA, USA, 1987; pp. 55–59.
- 92. Fan, Y.; Iwashita, T.; Egami, T. Energy landscape-driven non-equilibrium evolution of inherent structure in disordered material. *Nat. Comm.* **2017**, *8*, 15417. [CrossRef]

**Disclaimer/Publisher's Note:** The statements, opinions and data contained in all publications are solely those of the individual author(s) and contributor(s) and not of MDPI and/or the editor(s). MDPI and/or the editor(s) disclaim responsibility for any injury to people or property resulting from any ideas, methods, instructions or products referred to in the content.